6730 *Biochemistry* **2009,** *48,* 6730–6746
DOI: 10.1021/bi9000529

BIOCHEMISTRY
including biophysical chemistry & molecular biology
*Article*

# Mechanism of NTP Hydrolysis by the *Escherichia coli* Primary Replicative Helicase DnaB Protein. 2. Nucleotide and Nucleic Acid Specificities[†]

Anasuya Roychowdhury, Michal R. Szymanski, Maria J. Jezewska, and Wlodzimierz Bujalowski*

*Department of Biochemistry and Molecular Biology, Department of Obstetrics and Gynecology, and The Sealy Center for Structural Biology and Molecular Biophysics, Sealy Center for Cancer Cell Biology, The University of Texas Medical Branch at Galveston, 301 University Boulevard, Galveston, Texas 77555-1053*

*Received January 13, 2009; Revised Manuscript Received April 22, 2009*

ABSTRACT: The kinetic mechanism of NTP binding and hydrolysis by the *Escherichia coli* replicative helicase, the DnaB protein, in the absence and presence of the single-stranded DNA (ssDNA), has been quantitatively examined using the rapid quench-flow technique, under single-turnover conditions. In the case of both the free helicase and the enzyme−ssDNA complexes, the mechanism is independent of the type of base of the cofactor or the DNA; the bimolecular association is followed by the reversible chemical hydrolysis and subsequent conformational transition of the enzyme−product complex. The NTP hydrolysis step is significantly faster for the purine than for the pyrimidine cofactor, both in the absence and in the presence of the DNA. The temperature effect indicates that the nature of intermediates of the purine nucleotide, ATP, is different from the nature of the analogous intermediates of the pyrimidine nucleotide, CTP. Nevertheless, both types of cofactors seem to approach a similar "exit" state at the end of the reaction. The effect of ssDNA on the kinetics of NTP hydrolysis depends on the type of nucleotide cofactor and the base composition of the DNA and is centered at the hydrolysis step. Homoadenosine ssDNA oligomers are particularly effective in increasing the hydrolysis rate. The allosteric signal from the DNA, which activates the NTP hydrolysis, comes predominantly from the strong DNA-binding subsite. The role of the weak DNA-binding subsite is to modulate the allosteric effect of the strong subsite. The significance of these results for the mechanism of the free energy transduction by the DnaB helicase is discussed.

Helicases are motor proteins that utilize the energy from the nucleotide triphosphate binding and hydrolysis to perform unwinding of the duplex nucleic acid conformation and mechanical translocation along the nucleic acid lattice (*1*−*7*). The DnaB protein is the primary replication helicase in the *Escherichia coli* cell and is involved in both the initiation and elongation stages of chromosomal DNA replication, as well as in the replication of phage and plasmid DNA (*6*−*14*). It is the only helicase required to reconstitute DNA replication in vitro from the chromosomal origin of replication (oriC). The enzyme exists as a homohexamer in which six subunits form a ringlike structure, stabilized by magnesium cations (*15*−*19*). In the presence of ATP nonhydrolyzable analogues, i.e., in the stationary complex without ATP hydrolysis, the DnaB helicase binds the ssDNA[1] with a stoichiometry of 20 ± 3 nucleotides and the equilibrium DNA-binding site is located inside the cross channel of the hexamer (*18*−*25*). Although each subunit can bind the ssDNA, the DnaB hexamer effectively has a single total DNA-binding site. Nevertheless, the structure of the total DNA-binding site is heterogeneous. It contains the strong and the weak DNA-binding subsites, each occluding ∼10 nucleotides of the total DNA-binding site and differing in ssDNA affinity by more than 2 orders of magnitude (*24*, *25*).

Quantitative thermodynamic studies have established that the DnaB helicase has six nucleotide-binding sites, one on each subunit, which show ground-state preference for the purine cofactors (*26*−*30*). The nucleotide binding process is biphasic. Three cofactor molecules bind independently in the high-affinity phase, and the next three nucleotides bind in the low-affinity phase. The biphasic behavior of binding isotherms is a result of the negative cooperative interactions among binding sites (*26*, *29*). Single-turnover studies of ATP hydrolysis by a noninteracting, nucleotide-binding site of the helicase indicate that bimolecular association of ATP is followed by the reversible ATP hydrolysis and subsequent conformational transition of the enzyme−product complex (*31*). In excellent agreement with the stopped-flow kinetic results, the hydrolysis data indicate that part of the ATP binding energy originates from the induced structural

[†]This work was supported by National Institutes of Health Grant R01 GM-46679 (to W.B.).

*To whom correspondence should be addressed: Department of Biochemistry and Molecular Biology, The University of Texas Medical Branch at Galveston, 301 University Blvd., Galveston, TX 77555-1053. Telephone: (409) 772-5634. Fax: (409) 772-1790. E-mail: wbujalow@utmb.edu.

[1]Abbreviations: NTP, ribonucleoside triphosphate; GTP, guanosine triphosphate; GDP, guanosine diphosphate; CTP, cytidine triphosphate; CDP, cytidine diphosphate; Tris, tris(hydroxymethyl)aminomethane; AMP-PNP, $\beta,\gamma$-imidoadenosine 5′-triphosphate; ssDNA, single-stranded DNA; dsDNA, double-stranded DNA; $\varepsilon$A, ethenoadenosine.

 Published on Web 05/12/2009 

changes of the DnaB protein−ATP complex prior to ATP hydrolysis (*30*). The value of the partial equilibrium constant of the chemical interconversion, ATP ↔ ADP, is ∼2−5, indicating that the free energy of ATP hydrolysis is released from the enzyme−product complex in the conformational transitions of the intermediates, similar to the case of other motor proteins (*32*, *33*).

Elucidation of the nucleotide−DnaB helicase interactions, including the mechanism of NTP hydrolysis by the enzyme, is of paramount importance for understanding the different activities of the enzyme, including dsDNA unwinding and mechanical translocation. The role of preference for the purine cofactors in the mechanism of the cofactor hydrolysis and effectiveness of the free energy transduction in the dsDNA unwinding by the enzyme is unknown. Recall that the DnaB helicase acquires high ssDNA affinity only in the presence of ATP or ATP nonhydrolyzable analogues (*19*−*25*). Early qualitative studies have indicated that DNA significantly affects the steady-state ATPase activity of the DnaB helicase (*11*, *12*). In the companion paper (DOI 10.1021/bi900050x), we describe the presence of the allosteric effect of the bound nucleic acid on the helicase−cofactor interactions in the ground state, i.e., in the absence of NTP hydrolysis. However, how these allosteric interactions between the DNA- and nucleotide-binding sites affect the kinetics of NTP hydrolysis and the energetics of reaction intermediates is unknown. Nothing is known about the effect of the different base compositions of the nucleic acid on the mechanism and/or efficiency of NTP hydrolysis. The effects of the strong and weak DNA-binding subsites on the NTPase activity of the enzyme have never been examined.

In this work, we quantitatively and extensively examine the mechanisms and energetics of NTP binding and hydrolysis, in the presence and absence of ssDNA homo-oligomers differing in the type of base by a single, noninteracting site of the DnaB helicase. The kinetic mechanism of NTP binding and hydrolysis by the free helicase, as well as by the enzyme−ssDNA complexes, is independent of the type of base of the cofactor or the DNA. The NTP hydrolysis step is significantly faster for the purine than for the pyrimidine cofactors. Moreover, the nature of intermediates of the purine cofactor is different from the nature of the analogous intermediates of the pyrimidine cofactor. Nevertheless, both types of cofactors approach a similar "exit" state. The allosteric signal from the bound nucleic acid, which activates the NTP hydrolysis, comes predominantly from the strong DNA-binding subsite.

## MATERIALS AND METHODS

*Reagents and Buffers*. All solutions were made with distilled and deionized >18 MΩ (Milli-Q Plus) water. All chemicals were reagent grade. Buffer T4 is 50 mM Tris adjusted to pH 8.1 with HCl at 20 °C, containing 100 mM NaCl, 5 mM $MgCl_2$, 10% glycerol, and 1 mM DDT.

*DnaB Protein*. The *E. coli* DnaB protein was purified as previously described by us (*16*, *26*−*28*).

*Nucleotides and Nucleic Acids*. Radioactive [α-$^{32}$P]ATP, [α-$^{32}$P]GTP, and [α-$^{32}$P]CTP were from Amersham. Cold ATP, GTP, and CTP were from Sigma. The reaction mixture was prepared by mixing [α-$^{32}$P]NTP with cold NTP in a ratio of ∼1:19. We have determined that both radioactive and cold NTPs contained ∼5−6% of the material, comigrating with ATP, which could not be hydrolyzed even after being exposed at 100 °C in 6 M HCl for 6 h. The maximum extent of enzymatic hydrolysis in all kinetic experiments was corrected for the presence of the nonhydrolyzable material. All unmodified and fluorescein-labeled ssDNA oligomers were from Midland (Midland, TX). The concentration of the DNA oligomer, labeled at the 5′ end with fluorescein, 5′-Fl-dA(pA)$_{19}$, has been determined spectrophotometrically (*24*, *25*). The etheno derivatives of the ssDNA oligomers, dA(pA)$_{19}$, dA(pA)$_9$(pT)$_{10}$, and dT(pT)$_9$(pA)$_{10}$, were obtained by modification with chloroacetaldehyde (*18*−*20*, *25*, *34*−*37*). The concentration of the etheno derivative of the nucleic acids was determined using the extinction coefficient of ethenoadenosine, 3700 $M^{-1}$ $cm^{-1}$ (nucleotide), at 257 nm (*18*−*20*, *25*, *34*).

*Rapid Quench-Flow Kinetics*. Time courses of NTP hydrolyses by the DnaB helicase were determined using the rapid quench-flow instrument, RQF-3 (KinTek), as we previously described (*31*). Briefly, usually three points were collected and averaged for a given time interval. The reaction was quenched in 0.4 M EDTA (pH 8.1, 10% glycerol) (*31*). The product of the reaction, [α-$^{32}$P]NDP, was separated from [α-$^{32}$P]NTP using thin layer chromatography on polyethyleneimine (PEI)-cellulose (Merck) with 0.6 M potassium phosphate (pH 3.4) as the developing solution. As a reference, the original [α-$^{32}$P]NTP samples were also chromatographically analyzed on PEI-cellulose. The extent of hydrolysis was quantified using a phosphorimager SI (Molecular Dynamics) (*31*).

The kinetic measurements were performed in a large excess of DnaB helicase (single-turnover conditions) (*31*, *38*). The single-turnover kinetic curves were fitted to extract relaxation times and amplitudes using the nonlinear, least-squares fit routine (Mathematica, Wolfram, IL) with the exponential function defined as (*31*)

$$P(t) = P(\infty) + \sum_{i=1}^{n} A_i \exp(-\lambda_i t) \quad (1)$$

where $P(t)$ is the [α-$^{32}$P]NDP concentration at time $t$, $P(\infty)$ is the [α-$^{32}$P]NDP concentration at transient equilibrium, $A_i$ is the amplitude corresponding to the $i$th relaxation process, $\lambda_i$ is the time constant (reciprocal relaxation time, $1/\tau_i$) characterizing the $i$th relaxation process, and $n$ is the number of relaxation processes. All further analyses of the data were performed using Mathematica and Kaleida Graph (Synergy Software, Reading, PA) (*31*).

*Analytical Ultracentrifugation Measurements*. Sedimentation velocity experiments were performed with an Optima XL-A analytical ultracentrifuge (Beckman Inc., Palo Alto, CA) as described in the companion paper (DOI 10.1021/bi900050x). The sedimentation velocity scans were collected at the absorption band of the fluorescein residue (485 nm) (*24*, *25*).

*Fluorescence Measurements*. The steady-state fluorescence titrations were performed using the SLM-AMINCO 8100C instrument, as described in the companion paper (DOI 10.1021/bi900050x) (*18*−*25*). The binding of etheno derivatives of the ssDNA oligomers was monitored by following the fluorescence of the nucleic acids ($\lambda_{ex}$ = 325 nm; $\lambda_{em}$ = 410 nm). The relative fluorescence increase of the ssDNA, $\Delta F_{obs}$, upon the binding of the DnaB protein is defined as $\Delta F_{obs} = (F_i - F_o)/F_o$, where $F_i$ is the fluorescence of the DNA at a given titration point and $F_o$ is the initial value of the fluorescence of the sample.

## RESULTS

*Base Specificity of the DNA-Independent NTP Hydrolysis at a Single, Noninteracting Site on the DnaB Helicase*. Although the DnaB helicase can hydrolyze all NTPs, thermodynamic studies have indicated that the DnaB helicase has a significant ground-state preference for the purine cofactors,

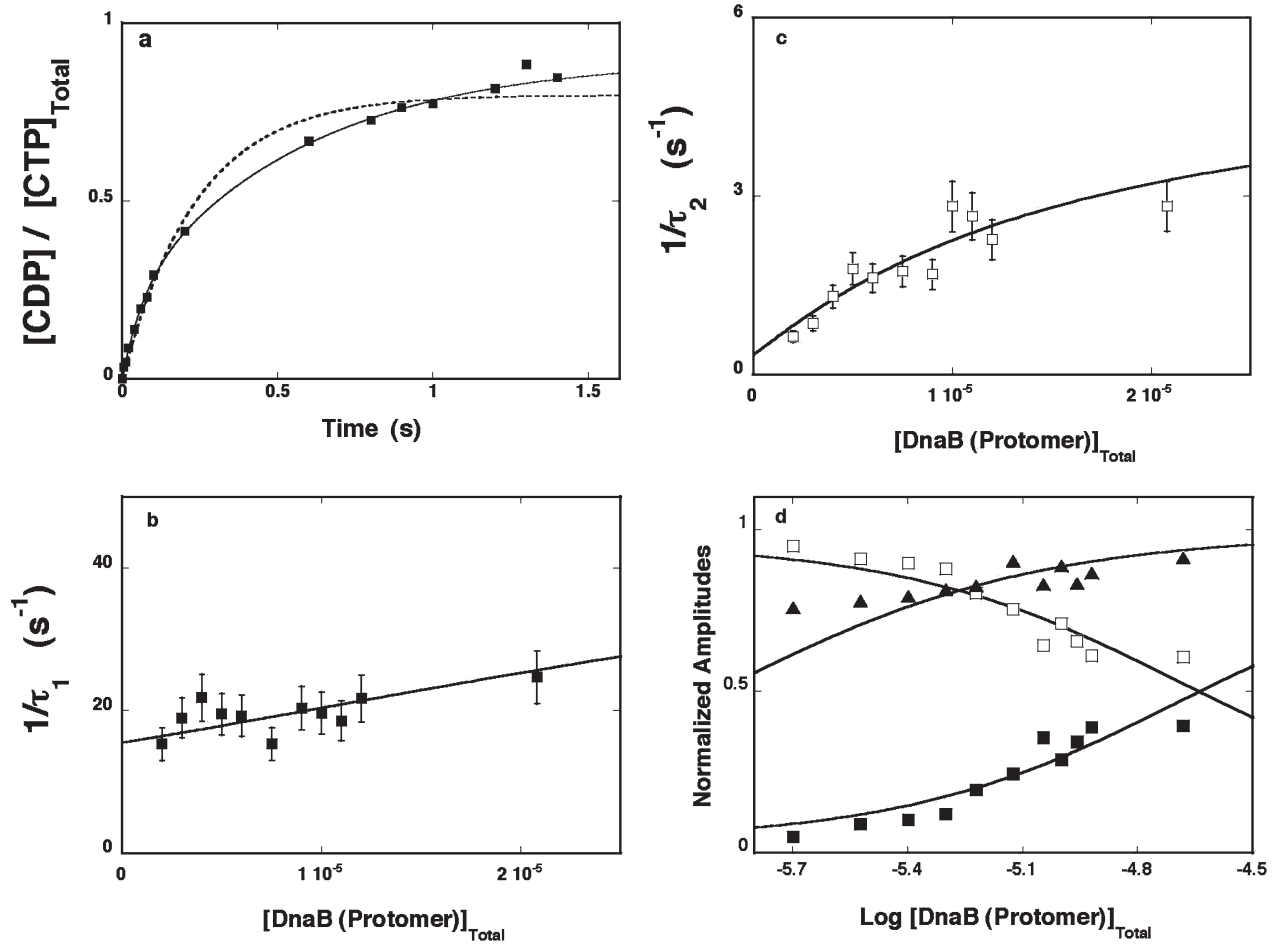


FIGURE 1: (a) Time course of CTP hydrolysis by a single, noninteracting site of the DnaB helicase hexamer in single-turnover experiments (large excess of the enzyme over CTP), in buffer T4. The produced CDP is shown as a fraction of the total concentration of CTP in the sample. The concentrations of the cofactor and the enzyme were $1.9 \times 10^{-7}$ M and $7.5 \times 10^{-6}$ M (protomer), respectively. The solid line is the nonlinear least-squares fit of the double-exponential function (eq 1) to the experimental kinetic curve. The dashed line is the nonlinear least-squares fit, obtained using a single-exponential function (eq 1) (details in the text). (b) Dependence of the reciprocal of the relaxation time, $1/\tau_1$, for CTP hydrolysis by the single, noninteracting site of the DnaB helicase in buffer T4, on the total concentration of the enzyme (protomer). The solid line is a numerical, nonlinear least-squares fit of the expenmental data to the three-step sequential mechanism, defined by Scheme 1. (c) Dependence of the reciprocal of the relaxation time, $1/\tau_2$, for CTP hydrolysis by the single, noninteracting site of the DnaB helicase in buffer T4, on the total concentration of the enzyme (protomer). The solid line is a numericnl, nonlinear least-squares fit of the experimental data to the three-step sequential mechanism, defined by Scheme 1. The error bars in panels b and c are standard deviations determined in three or four independent experiments. (d) Dependence of the normalized total and individual relaxation amplitudes, $A_T$ (▲), $A_1$ (■), and $A_2$ (□), of CTP hydrolysis by a single, noninteracting site of the DnaB helicase in buffer T4 on the total concentration of the enzyme (protomer). The solid lines are nonlinear least-squares fits according to the three-step sequential mechanism of ATP hydrolysis in the noninteracting site of the helicase, described by Scheme 1. The rate constants, obtained from the fits of the relaxation times and the amplitudes, are included in Table 1.

as compared to pyrimidine nucleotides (*20*). To address mechanistic differences in the observed preference, we performed single-turnover studies of the NTPs differing by the type of the base. A rapid quench-flow kinetic curve of [α-$^{32}$P]CTP hydrolysis after mixing $1.9 \times 10^{-7}$ M CTP with the DnaB helicase ($7.5 \times 10^{-6}$ M) (protomer) (final concentrations) in buffer T4 is shown in Figure 1a. The product formation, [α-$^{32}$P]CDP, is shown as a molar fraction of the total concentration of [α-$^{32}$P]CTP, i.e., [[α-$^{32}$P]CDP]/[[α-$^{32}$P]CTP]. At the applied, total concentration of CTP, only a single site of the DnaB helicase interacts with the cofactor (*20*). There are two important qualitative aspects of the observed kinetic curve (*31*). First, the plateau does not reach the maximum possible value of the total CTP concentration. The same plateau is reached at the higher enzyme concentrations (data not shown), indicating that, in the studied time range, the helicase−CTP system reaches an effective, transient equilibrium in the active site (*31*). Second, there is no detectable time lag in the appearance of the reaction product. As we discussed before, such behavior strongly indicates that one simultaneously observes at least two species containing [α-$^{32}$P]CDP (*31*).

The solid line in Figure 1a is a nonlinear least-squares fit of the experimental curve, using eq 1 with a double-exponential function. The dashed line is a corresponding single-exponential linear least-squares fit. It is evident that only the double-exponential fit adequately represents the observed experimental curve, although we cannot exclude the presence of additional steps, whose detection is hindered by the limited resolution of the rapid quench-flow technique. The reciprocal relaxation times, $1/\tau_1$ and $1/\tau_2$, as functions of the total DnaB helicase concentration (protomer), are shown in panels b and c of Figure 1 (*30*, *31*, *39*−*43*). The value of $1/\tau_1$ increases linearly with DnaB concentration. The values of $1/\tau_2$ show a hyperbolic dependence upon the DnaB concentration, indicating that it describes an intramolecular isomerization process (*31*, *39*−*43*). Though the linear dependence of the short relaxation time as a function of $[DnaB]_T$ (Figure 1b) suggests that it could describe a bimolecular process, the behavior

Table 1: Thermodynamic and Kinetic Parameters of the NTP Hydrolysis by the DnaB Helicase, in a Single Turnover, in the Absence and Presence of Different ssDNA Oligomers, in Buffer T2 (pH 8.1 and 20 °C) (see the text for details)[a]

| complex | $K_1$ ($M^{-1}$) | $K_2$ | $K_3$ | $k_2$ ($s^{-1}$) | $k_{-2}$ ($s^{-1}$) | $k_3$ ($s^{-1}$) | $k_{-3}$ ($s^{-1}$) |
|---|---|---|---|---|---|---|---|
| DnaB−ATP | $(1.6 \pm 0.5) \times 10^4$ | $5.0 \pm 1.6$ | $12.3 \pm 4$ | $258 \pm 36$ | $52 \pm 8$ | $12.3 \pm 1.9$ | $1.0 \pm 0.10$ |
| DnaB−ATP−dA$(pA)_{19}$ | $(4.0 \pm 1.3) \times 10^4$ | $3.9 \pm 1.3$ | $21.7 \pm 9.1$ | $\geq 2700$ | $\geq 700$ | $7.6 \pm 1.1$ | $0.35 \pm 0.05$ |
| DnaB−ATP−dC$(pC)_{19}$ | $(1.0 \pm 0.3) \times 10^5$ | $1.7 \pm 0.6$ | $37 \pm 12$ | $39 \pm 8$ | $23 \pm 3$ | $11 \pm 2$ | $0.30 \pm 0.05$ |
| DnaB−ATP−dT$(pT)_{19}$ | $(1.0 \pm 0.3) \times 10^5$ | $1.3 \pm 0.4$ | $32 \pm 11$ | $90 \pm 14$ | $72 \pm 11$ | $16 \pm 2$ | $0.50 \pm 0.10$ |
| DnaB−GTP | $(1.3 \pm 1.2) \times 10^4$ | $12.2 \pm 1.6$ | $7.3 \pm 2.7$ | $220 \pm 18$ | $21 \pm 3$ | $8.0 \pm 1.2$ | $1.1 \pm 0.20$ |
| DnaB−GTP−dA$(pA)_{19}$ | $(8.0 \pm 0.9) \times 10^4$ | $3.4 \pm 1.1$ | $30 \pm 9$ | $\geq 2400$ | $\geq 800$ | $4.5 \pm 1.1$ | $0.20 \pm 0.05$ |
| DnaB−GTP−dC$(pC)_{19}$ | $(2.1 \pm 0.7) \times 10^4$ | $2.2 \pm 0.8$ | $93 \pm 31$ | $620 \pm 93$ | $280 \pm 42$ | $28 \pm 4$ | $0.30 \pm 0.05$ |
| DnaB−GTP−dT$(pT)_{19}$ | $(2.6 \pm 0.9) \times 10^4$ | $2.6 \pm 0.9$ | $40 \pm 13$ | $160 \pm 24$ | $61 \pm 9$ | $24 \pm 4$ | $0.60 \pm 0.10$ |
| DnaB−CTP | $(9.1 \pm 0.7) \times 10^3$ | $8.4 \pm 2.4$ | $10.4 \pm 3.8$ | $83 \pm 12$ | $9.9 \pm 1.5$ | $5.5 \pm 0.9$ | $0.5 \pm 0.10$ |
| DnaB−CTP−dA$(pA)_{19}$ | $(1.3 \pm 0.4) \times 10^4$ | $4.2 \pm 1.4$ | $25 \pm 8$ | $400 \pm 60$ | $95 \pm 14$ | $7.5 \pm 1.1$ | $0.30 \pm 0.05$ |
| DnaB−CTP−dC$(pC)_{19}$ | $(1.7 \pm 0.6) \times 10^4$ | $2.5 \pm 0.9$ | $27.1 \pm 9$ | $50 \pm 8$ | $20 \pm 3$ | $19 \pm 3$ | $0.70 \pm 0.10$ |
| DnaB−CTP−dT$(pT)_{19}$ | $(1.0 \pm 1.1) \times 10^4$ | $4.4 \pm 1.4$ | $11.4 \pm 3.5$ | $114 \pm 14$ | $26 \pm 4$ | $10.3 \pm 1.3$ | $0.80 \pm 0.10$ |
| DnaB−CTP−dA$(pA)_9(pC)_{10}$ | $(1.4 \pm 0.4) \times 10^4$ | $1.9 \pm 0.6$ | $57 \pm 19$ | $\geq 1700$ | $\geq 900$ | $17 \pm 2.3$ | $0.30 \pm 0.10$ |
| DnaB−CTP−dC$(pC)_9(pA)_{10}$ | $(1.4 \pm 0.4) \times 10^4$ | $1.9 \pm 0.6$ | $67 \pm 22$ | $170 \pm 25$ | $90 \pm 16$ | $20 \pm 3$ | $0.30 \pm 0.10$ |

[a] Errors are standard deviations determined using three or four independent experiments.

of the amplitudes of both relaxation processes indicates a more complex mechanism (*31*). The dependence of the individual amplitudes, $A_1$ and $A_2$, of the observed relaxation steps upon the logarithm of the DnaB protein concentration (protomer) is shown in Figure 1d. The absolute values of individual amplitudes are normalized, i.e., expressed as fractions of the total amplitude, $A_i/\sum A_i$. At low helicase concentrations, the slowest relaxation process (amplitude $A_2$) dominates the observed total amplitude. As the concentration of the DnaB helicase increases, the amplitude of the faster normal mode, $A_1$, increases and at high enzyme concentrations approaches the value of $A_2$. The total amplitude, $A_T$, gradually increases as $[DnaB]_T$ increases. Such behavior of the relaxation amplitudes and the lack of the time lag in the kinetic curves indicate that both relaxation processes reflect intramolecular transitions of the formed complex (*39*−*43*). The linear apparent dependence of $1/\tau_1$ upon [DnaB] results from the low affinity of the cofactor in the first bimolecular binding step, i.e., only the initial part of the true hyperbolic dependence is observed in the experiment (*31*, *39*−*43*).

The simplest mechanism of the CTP hydrolysis by the DnaB helicase, which can account for the observed experimental behavior, is, in general, described by Scheme 1 A bimolecular association of the cofactor with the active site of one of the DnaB subunits (H + CTP ↔ H-CTP) is followed by two reversible first-order transitions, the CTP hydrolysis [H-CTP ↔ (H-CDP·$P_i$)$_1$] and the isomerization of the helicase−product complex [(H-CDP·$P_i$)$_1$ ↔ (H-CDP·$P_i$)$_2$] (*31*). Thus, the major aspects of the kinetic mechanism of the pyrimidine cofactor hydrolysis, CTP, are the same as the main features of the ATP kinetic mechanism (*31*). The solid lines in panels b−d of Figure 1b are nonlinear least-squares fits of the relaxation times and amplitudes according to the proposed mechanism (Scheme 1). The analyses were first performed by numerical, nonlinear least-squares fitting of the individual relaxation times and amplitudes, using the matrix projection operator approach (*40*). Simultaneous, global fitting of both the relaxation times and the amplitudes then refined the values of the rate constants. The obtained rate and equilibrium constants are included in Table 1.

Rapid quench-flow kinetic curves of [α-$^{32}$P]ATP and [α-$^{32}$P]GTP hydrolysis, after $1.9 \times 10^{-7}$ M NTP had been mixed with the DnaB helicase ($7.5 \times 10^{-6}$ M) (protomer) (final concentrations) in buffer T4, are shown in Figure 2. For the sake of comparison, the kinetic curve of [α-$^{32}$P]CTP, obtained at the same enzyme concentration, is also included in Figure 2. The product formations, [α-$^{32}$P]NDP, are shown as molar fractions of the total concentration of [α-$^{32}$P]NTP (see above). The data in Figure 2 show that the rate of product formation is significantly faster for the purine cofactors than for the pyrimidine nucleotide (see below). The solid lines in Figure 2 are nonlinear least-squares fits of the experimental curves, using eq 1, with the double-exponential function. The single-exponential fit does not provide adequate description of the observed behavior (Figure 1a). The analyses of the determined reciprocal relaxation times, $1/\tau_1$ and $1/\tau_2$, and amplitudes, $A_1$, $A_2$, and $A_T$, as functions of the DnaB helicase concentration (protomer) have been performed as described above (data not shown). The determined values of the partial equilibrium and rate constants are included in Table 1.

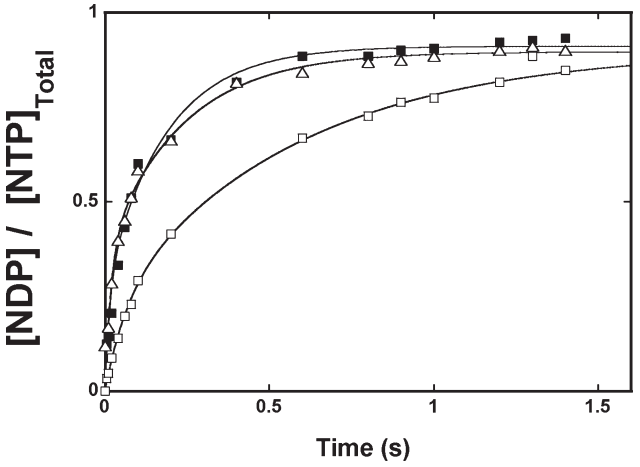


FIGURE 2: Time course of ATP (■), CTP (□), and GTP (△) hydrolysis by a single, noninteracting site of the DnaB helicase hexamer in single-turnover experiments in buffer T4. The produced NDPs (ADP, CDP, and GDP) are shown as fractions of the total concentration of the corresponding NTPs (ATP, CTP, and GTP) in the sample. The concentrations of the cofactors were $1.9 \times 10^{-7}$ M. The concentration of the enzyme was $7.5 \times 10^{-6}$ M (protomer). The solid lines are the nonlinear least-squares fits of the double-exponential function (eq 1) to the experimental kinetic curves (details in the text).

The obtained data indicate that all examined cofactors have similar values of the partial equilibrium constants, $K_1$, $K_2$, and $K_3$, characterizing the internal equilibria between different intermediates of the reaction, described by Scheme 1 (Table 1). The bimolecular association process (H + NTP ↔ H-NTP) is too

fast to be accessed in a rapid quench-flow experiment. However, the value of $K_1$, which characterizes the formation of the first intermediate, H-NTP, can be obtained and is lower for CTP than for ATP and GTP. Nevertheless, the affinity difference is less pronounced than has been determined in the thermodynamic studies of the ground-state interactions, i.e., in the absence of the chemical step (*26*−*29*) (see Discussion). The values of $K_2$ are low for all cofactors, indicating that there is no significant release of the free energy of the nucleotide hydrolysis in this step (*31*−*33*, *44*). The rate constants, $k_3$ and $k_{-3}$, for the slowest intramolecular transition and resulting values of $K_3$ ($=k_3/k_{-3}$) are also similar for all cofactors. Nevertheless, the major difference between CTP and purine cofactors, ATP and GTP, is in the rate constants characterizing the hydrolysis step, $k_2$ and $k_{-2}$. Both forward and backward rate constants for the hydrolysis step for the purine nucleotides are significantly larger than those observed for the pyrimidine cofactor (Table 1) (see Discussion).

*Effect of Temperature on the ATP and CTP Hydrolysis by the Single, Noninteracting Site on the DnaB Helicase.* To further address the differences between the purine and pyrimidine cofactors, we performed single-turnover analysis of the ATP and CTP hydrolyses by the DnaB helicase as a function of temperature. Figure 3a shows the dependence of the natural logarithms of the partial equilibrium constants, characterizing the formation of the DnaB−ATP intermediates, as a function of the reciprocal temperature (kelvin) (van't Hoff plots). The corresponding van't Hoff plots for the DnaB complex with the CTP cofactor are shown in Figure 3b. All plots are, within experimental accuracy, linear in the studied temperature range. However, the behavior of the partial equilibrium constants, as a function of temperature, is very different for ATP and CTP. In the case of the purine cofactor, the value of $K_1$ decreases while the values of $K_2$ and $K_3$ increase with an increase in temperature. An opposite behavior is observed for CTP. The value of $K_1$ increases while the values of $K_2$ and $K_3$ decrease with an increase in temperature. The obtained apparent enthalpies and entropies ($\Delta H_i$ and $\Delta S_i$, respectively) of the individual intermediate formations (Scheme 1) are included in Table 2.

The differences between thermodynamic functions characterizing the equilibria among the intermediates of the DnaB−NTP hydrolysis reaction for the purine versus pyrimidine cofactors are striking. In the case of the purine cofactor, the bimolecular step (H + NTP ↔ H-NTP) is an enthalpy-driven process ($\Delta H_1 \approx -18.4$ kcal/mol) and accompanied by a large, apparent negative entropy change ($\Delta S_1 \approx -44$ cal mol$^{-1}$ °C$^{-1}$). Such large values of thermodynamic functions indicate that the observed bimolecular process must include an additional step(s), which is beyond the resolution of the rapid quench-flow experiment (see Discussion). Both subsequent steps, the chemical hydrolysis [H-NTP ↔ (H-NDP·P$_i$)$_1$] and the following conformational transition [(H-NDP·P$_i$)$_1$ ↔ (H-NDP·P$_i$)$_2$], are endothermic processes, driven by apparent positive entropy changes. In the complex with the pyrimidine cofactor, the bimolecular binding process is endothermic and driven by a large, apparent positive entropy change ($\Delta S_1 \approx 53$ cal mol$^{-1}$ °C$^{-1}$). The two subsequent steps are both exothermic and accompanied by modest negative entropy changes (Table 2) (see Discussion).

*Effect of Different ssDNA Homo-Oligomers on the ATP Hydrolysis Reaction Catalyzed by the DnaB Helicase.* Examination of the NTP hydrolysis by the DnaB helicase−ssDNA complex is rendered difficult by the fact that the enzyme acquires strong ssDNA affinity only in the presence of ATP or

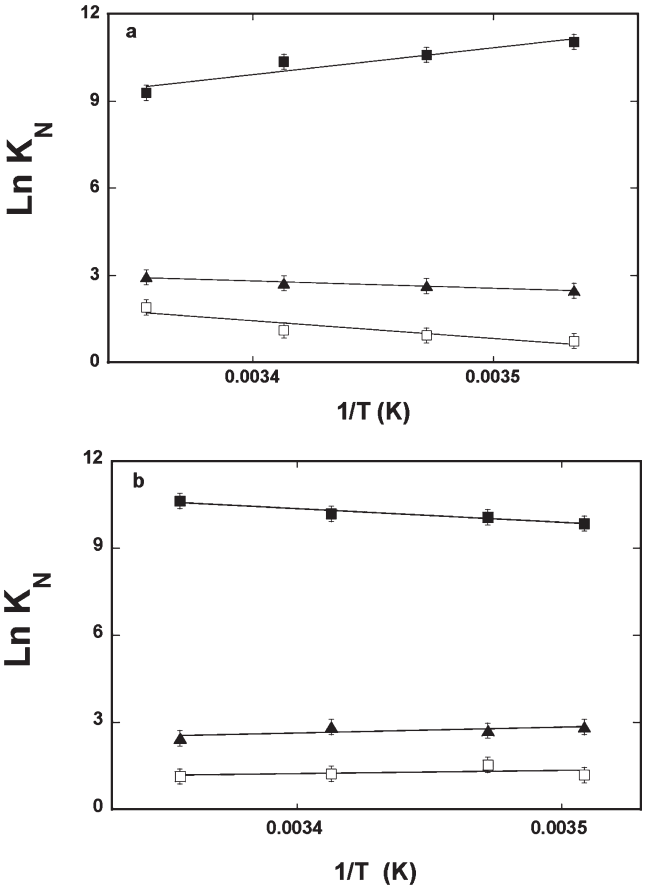


FIGURE 3: (a) Dependence of the partial equilibrium constants, characterizing the equilibria between the intermediates of the ATP hydrolysis reaction by the single, noninteracting site of the DnaB helicase, on the reciprocal of the temperature (kelvin) (van't Hoff plots): $K_1$ (■), $K_2$ (□), and $K_3$ (▲). (b) Dependence of the partial equilibrium constants, characterizing the equilibria between the intermediates of the CTP hydrolysis reaction by the single, noninteracting site of the DnaB helicase, on the reciprocal of the temperature (kelvin) (van't Hoff plots): $K_1$ (■), $K_2$ (□), and $K_3$ (▲). The obtained values of corresponding enthalpy and entropy changes are included in Table 2.

ATP nonhydrolyzable analogues (*26*−*29*). Nevertheless, we have found that the helicase possesses the ssDNA affinity, even in the absence of the nucleotide cofactors. To address the binding of the DnaB hexamer to the ssDNA in the absence of the cofactors, we applied the sedimentation velocity technique, as analogously described in our previous studies of various protein−DNA complexes (*23*, *45*−*47*). We utilize the fact that the sedimentation coefficient of the DnaB hexamer (~10.8 S) is much larger than the sedimentation coefficient of the modified ssDNA 20-mer, 5′-Fl-dA(pA)$_{19}$ (~1.3 S), which contains fluorescein at its 5′ end (Materials and Methods). Therefore, in our experimental design, the sedimentation of the nucleic acid can be exclusively monitored at the fluorescein absorption band (485 nm) without any interference from the protein absorbance. The formation of the complex between the ssDNA oligomer and the DnaB helicase is manifested by a large increase of the apparent sedimentation coefficient of the ssDNA 20-mer associated with the enzyme (*45*−*47*). In previous studies, we have determined that the presence of fluorescein does not affect, to any detectable extent, the affinity of the ssDNA for the DnaB helicase (*27*, *28*).

Sedimentation velocity profiles of 5′-Fl-dA(pA)$_{19}$, in the presence of the DnaB hexamer and in the absence of a nucleotide cofactor, are shown in Figure 4. The profiles have been recorded

Table 2: van't Hoff Enthalpies and Entropies Characterizing the Formation of Different Intermediates in the ATP and CTP Hydrolysis by the DnaB Helicase, in a Single Turnover, in Buffer T4 (pH 8.1 and 20 °C) (see the text for details)

| complex | $\Delta H_1$ (kcal/mol) | $\Delta S_1$[a](cal mol$^{-1}$ °C$^{-1}$) | $\Delta H_2$ (kcal/mol) | $\Delta S_2$[a](cal mol$^{-1}$ °C$^{-1}$) | $\Delta H_3$ (kcal/mol) | $\Delta S_3$[a](cal mol$^{-1}$ °C$^{-1}$) |
|---|---|---|---|---|---|---|
| DnaB−ATP | −18.4 ± 6.1 | −44 ± 15 | 12.1 ± 40 | 45 ± 15 | 5.0 ± 1.6 | 22 ± 7 |
| DnaB−CTP | 9.3 ± 3.1 | 52 ± 17 | −2.3 ± 0.7 | −5.4 ± 1.8 | −4.0 ± 1.3 | −8.0 ± 2.6 |

[a] Calculated using equilibrium constants $K_1$, $K_2$, and $K_3$ obtained at 20 °C.

at the fluorescein absorption band (485 nm). The total 20-mer and protein concentrations were $3 \times 10^{-6}$ M and $3 \times 10^{-5}$ M (hexamer), respectively. Thus, the helicase is in a large excess over the nucleic acid. The time interval between the scans is 10 min. At the same enzyme concentration and in the presence of the ATP nonhydrolyzable analogue AMP-PNP, the enzyme completely saturates the ssDNA oligomer (*18*−*20*). This is not the case here. The fast-moving boundary in Figure 4 corresponds to the 20-mer−DnaB hexamer complex. The very slow-moving boundary, at the applied rotational speed, corresponds to the sedimentation of the free 5′-Fl-dA(pA)$_{19}$. Thus, it is evident that the DnaB helicase can bind to the ssDNA, even in the absence of the nucleoside triphosphates. Nevertheless, the affinity is much lower than that observed in the presence of ATP nonhydrolyzable analogues, as at this high concentration of the protein, only a fraction of the nucleic acid is bound to the enzyme (Figure 4). However, the power of the applied sedimentation velocity approach is that one does not need to saturate the nucleic acid, or any ligand for that matter, to estimate the binding constant or stoichiometry of the formed complex [see below and the companion paper (DOI 10.1021/bi900050x)] (*45*−*47*).

From the plot, analogous to the one shown in Figure 4 and the known total concentration of the ssDNA 20-mer, [5′-Fl-dA(pA)$_{19}$]$_T$, one can estimate the macroscopic binding constant, $K$, of the DnaB helicase for the nucleic acid, in the absence of the cofactor. Using the total absorption, $T$, of 5′-Fl-dA(pA)$_{19}$ for the initial scans, which corresponds to the total concentration of the ssDNA oligomer, and the absorption of the slow moving boundary, $F$, one can directly calculate the absorption of the 5′-Fl-dA(pA)$_{19}$ bound to the helicase as $C = T - F$. Thus, the concentration of the ssDNA oligomer bound to the DnaB protein is $C/T \times$ [5′-Fl-dA(pA)$_{19}$]$_T$. The determined total average degree of binding of the DnaB protein on the ssDNA 20-mer is then $\sum\Theta_{Ni} = C/T$. Because only one ssDNA 20-mer can bind to the DnaB helicase, the total average degree of binding is related to the macroscopic binding constant, $K$, and the total DnaB concentration, [DnaB(hexamer)]$_T$, by the expression

$$K = \frac{\sum\Theta_{Ni}}{[\text{DnaB(hexamer)}]_T(1 - \sum\Theta_{Ni})} \quad (2)$$

The use of [DnaB(hexamer)]$_T$ instead of the free helicase concentration in eq 2 is justified by the fact that [DnaB(hexamer)]$_T \gg$ [5′-Fl-dA(pA)$_{19}$]$_T$; i.e., the free DnaB concentration is practically equal to the total concentration of the protein. The sedimentation velocity data in Figure 4 provide a $K$ value of $(3 \pm 1) \times 10^4$ M$^{-1}$. Once the value of the binding constant is known, we can estimate the concentration of the unmodified ssDNA 20-mer, dA(pA)$_{19}$, which is necessary to have as much as possible of the DnaB protein associated with the nucleic acid, in the absence of the nucleotide cofactor and still avoid precipitation of the complex. The optimal concentration of dA(pA)$_{19}$ is $6.5 \times 10^{-5}$ M (oligomer), at which ~65% of the protein is initially saturated

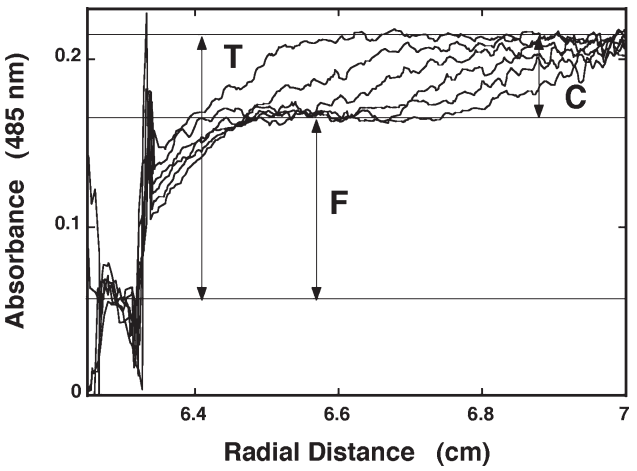


FIGURE 4: Sedimentation velocity absorption profiles, recorded at 485 nm, of the ssDNA 20-mer, 5′-Pl-dA(pA)$_{19}$, in the presence of the DnaB helicase in buffer T4, in the absence of nucleotide cofactors. The concentrations of the nucleic acid and the helicase were $3 \times 10^{-6}$ M (oligomer) and $3 \times 10^{-5}$ M (hexamer), respectively. The scans were collected at 30000 rpm. The short initial parts of the scans correspond to the buffer−air region above the sample meniscus. The arrows indicate the absorption of the total concentration of 5′-Fl-dA(pA)$_{19}$ ($T$), the concentration of the 20-mer bound to the DnaB helicase ($C$), and the concentration of the free 20-mer ($F$). The horizontal lines indicate the locations of the plateaus corresponding to the zero line, free, 5′-Fl-dA(pA)$_{19}$, concentration and the total, 5′-Fl-dA(pA)$_{19}$, concentration (see the text for details).

with the nucleic acid (see below). The fact that a significant part of the protein population is still not associated with the DNA does not affect the interpretation of the kinetics. This is because, at the selected protein and 20-mer concentrations, the high-affinity binding of the nucleic acid to the fraction of the DnaB helicase, associated with the nucleotide triphosphate in the single-turnover experiment, is very fast, and in analogy to the bimolecular step involving the NTP binding, this ssDNA binding step is not accompanied by any detectable amplitude (see below) (*30*, *31*, *40*).

A rapid quench-flow kinetic curve of [α-$^{32}$P]ATP hydrolysis, after $1.9 \times 10^{-7}$ M ATP had been mixed with the DnaB helicase ($7 \times 10^{-6}$ M) (protomer) and the ssDNA oligomer, dA(pA)$_{19}$ [$6.5 \times 10^{-5}$ M (oligomer)] (final concentrations) in buffer T4, is shown in Figure 5a. For the sake of comparison, the analogous kinetic curve obtained in the absence of the nucleic acid is included in Figure 5a. The presence of dA(pA)$_{19}$ has a dramatic effect on the observed product formation. Not only the rate of the bimolecular step but also the rate of the hydrolysis step, readily observed in the absence of the homoadenosine 20-mer, is beyond the time resolution of the rapid quench-flow technique. The solid line in Figure 5a is a nonlinear least-squares fit of the experimental curve using eq 1, with a single-exponential function. Only a single relaxation time, $1/\tau_2$, characterizing the slowest kinetic process, can be extracted from the data. The dependence of $1/\tau_2$ upon the DnaB helicase concentration (protomer) is shown in Figure 5b. The hyperbolic shape of the plot indicates that it

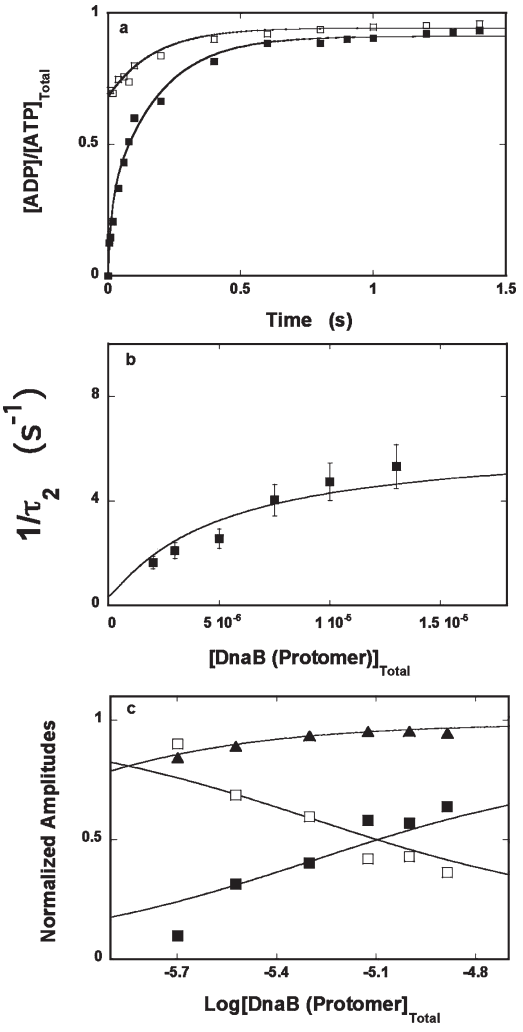


FIGURE 5: (a) Time course of ATP hydrolysis by a single, noninteracting site of the DnaB helicase hexamer in the presence of the ssDNA 20-mer, $dA(pA)_{19}$ (□), in single-turnover experiments, in buffer T4. The produced ADP is shown as a fraction of the total concentration of the ATP in the sample. The concentrations of the cofactor and the enzyme were $1.9 \times 10^{-7}$ M and $7.5 \times 10^{-6}$ M (protomer), respectively. The concentration of the nucleic acid was $6.5 \times 10^{-5}$ M (oligomer). For the sake of comparison, the time course of ATP hydrolysis by a single, noninteracting site of the DnaB helicase hexamer in the absence of the ssDNA 20-mer is included in panel a, obtained at the same cofactor and enzyme concentrations (■). The solid line is the nonlinear least-squares fit of the double-exponential function (eq 1) to the experimental curve (details in text). (b) Dependence of the reciprocal of the relaxation time, $1/\tau_2$, for ATP hydrolysis by the single, noninteracting site of the DnaB helicase, in the presence of $dA(pA)_{19}$ upon the total concentration of the enzyme (protomer). The solid line is a numerical, nonlinear least-squares fit of the experimental data to the three-step sequential mechanism, defined by Scheme 1. (c) Dependence of the normalized total and individual relaxation amplitudes, $A_T$ (▲), $A_1$ (■), and $A_2$ (□), of ATP hydrolysis by a single, noninteracting site of the DnaB helicase, in the presence of $dA(pA)_{19}$, on the logarithm of the total concentration of the enzyme (protomer). The solid lines are nonlinear least-squares fits according to the three-step sequential mechanism of ATP hydrolysis in the noninteracting site of the helicase, described by Scheme 1. The rate constants, obtained from the fits of the relaxation times and the amplitudes, are included in Table 1.

described an intramolecular transition. Although $\tau_1$ cannot be determined, the amplitude of the hydrolysis step, $A_1$, can be obtained as a difference ($A_1 = A_T - A_2$) (*31*). The dependencies of the normalized total, $A_T$, and individual amplitudes, $A_1$ and $A_2$, of the observed relaxation processes upon the logarithm of the DnaB protein concentration (protomer) are shown in Figure 5c. The plots are analogous to the behavior of the amplitudes in Figure 1d, indicating that both relaxation processes reflect intramolecular transitions of the formed complex and Scheme 1 describes the simplest mechanism of the observed reaction (*31*). There are only three amplitudes and a single relaxation time available from the experiments. Thus, it seems that we can directly determine only the product, $K_1K_2$, for the two fast steps. However, because the values of the amplitude of the bimolecular step are very low and beyond detection in the rapid quench-flow measurements, the amplitude of the fast step in Figure 5a directly indicates the equilibrium ratio of ATP and ADP prior to the slow step of the reaction (*31*, *41*). This allows us to estimate the value of $K_2$ and, in turn, the value of $K_1$ for ATP, using the product $K_1K_2$. The solid lines in panels b and c of Figure 5 are nonlinear least-squares fits of the relaxation times and amplitudes according to the mechanism, defined by Scheme 1. The obtained rate and equilibrium constants are included in Table 1.

A rapid quench-flow kinetic curve of [α-$^{32}$P]ATP hydrolysis, after $1.9 \times 10^{-7}$ M ATP had been mixed with the DnaB helicase ($7 \times 10^{-6}$ M) (protomer) and the ssDNA oligomer, $dC(pC)_{19}$ [$6.5 \times 10^{-5}$ M (oligomer)] (final concentrations) in buffer T4, is shown in Figure 6a. For the sake of comparison, the analogous kinetic curve obtained in the absence of the nucleic acid is included in Figure 6a. Contrary to the dramatic effect observed for $dA(pA)_{19}$, the presence of $dC(pC)_{19}$ has little effect on the observed ADP formation. Only the total amplitude of the ADP formation is slightly increased, as compared to the kinetic curve obtained in the absence of the nucleic acid (Figure 6a). The solid line in Figure 6a is a nonlinear least-squares fit of the experimental curve using the double-exponential function (eq 1), which provides an excellent description of the experimental data. The dependencies of the reciprocal relaxation times, $1/\tau_1$ and $1/\tau_2$, as well as the amplitudes, $A_T$, $A_1$, and $A_2$, as a function of the enzyme concentration, are shown in panels b–d of Figure 6. Both reciprocal relaxation times exhibit a hyperbolic dependence upon $[DnaB]_T$ (protomer), indicating that they describe intramolecular isomerization processes (*40*–*43*). In the case of the amplitudes, the slowest relaxation process (amplitude $A_2$) dominates the observed total amplitude, at low helicase concentrations. With an increasing concentration of the enzyme, the amplitude of the faster normal mode, $A_1$, increases and the total amplitude, $A_T$, increases. Thus, the behavior of all examined relaxation parameters indicates that the kinetic mechanism of ATP hydrolysis, in the presence of $dC(pC)_{19}$, is described by Scheme 1.

The obtained rate and equilibrium constants for the ATP hydrolysis by the DnaB helicase, in the presence of all examined ssDNA oligomers, are included in Table 1. The value of the partial equilibrium constant, $K_1$, is significantly larger in the presence of the nucleic acids, although much lower than expected on the basis of direct thermodynamic studies of the corresponding stationary complexes [companion paper (DOI 10.1021/bi900050x)] (*16*, *29*) (see Discussion). The partial equilibrium constant, $K_2$, which describes the chemical step [H-ATP ↔ (H-ADP·$P_i$)$_1$] is, in fact, decreased in the presence of the studied ssDNA oligomers, while the values of $K_3$ are increased, indicating that the transition of the enzyme–product complex, following the chemical step, is energetically more favorable. However, in spite of the similar values of $K_2$, the ssDNA homo-oligomers, containing cytidine and thymine, differ dramatically in their effect on the rate constants of the ATP hydrolysis, as compared

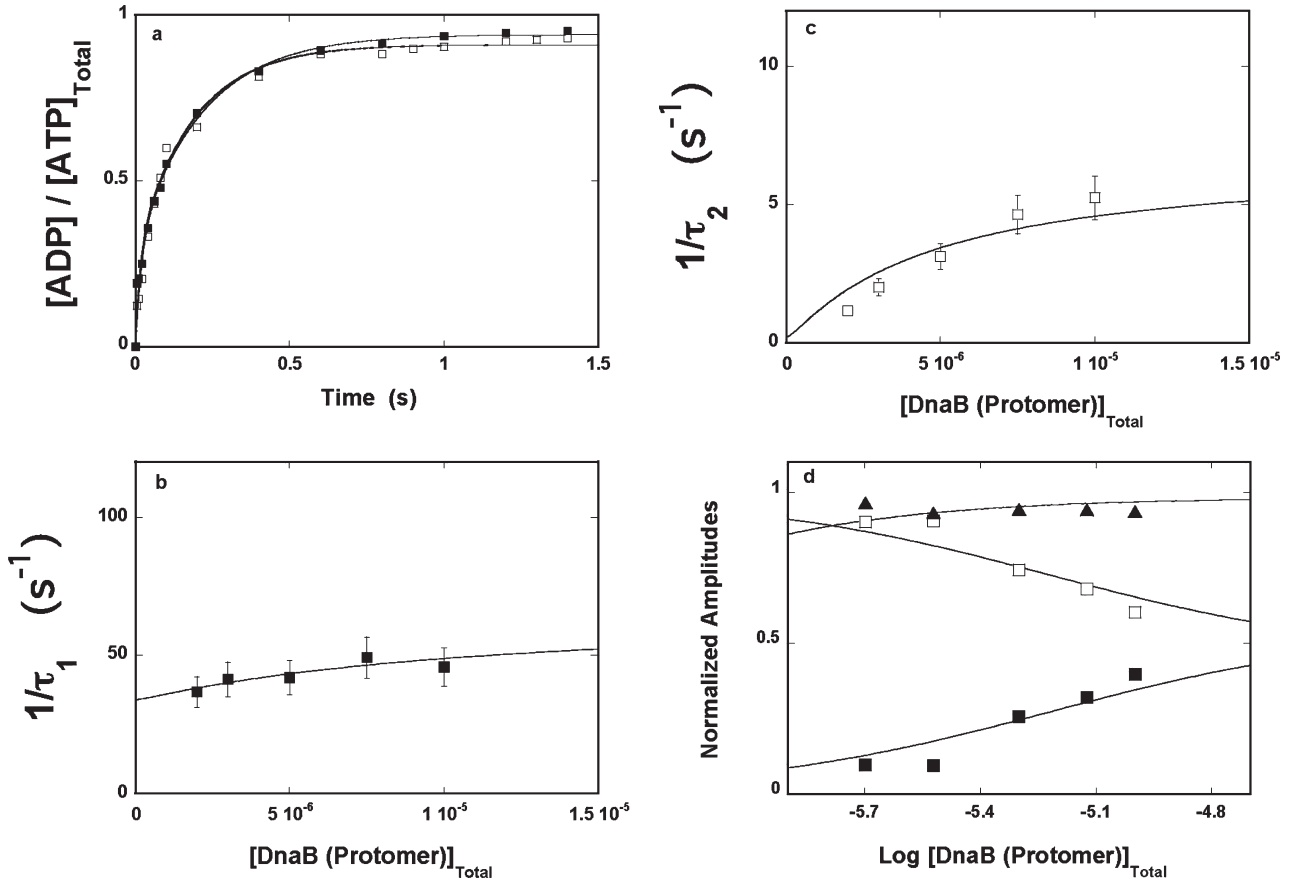


FIGURE 6: (a) Time course of ATP hydrolysis by a single, noninteracting site of the DnaB helicase hexamer in the presence of the ssDNA 20-mer, $dC(pC)_{19}$ (■), in single-turnover experiments, in buffer T4. The produced ADP is shown as a fraction of the total concentration of the ATP in the sample. The concentrations of the cofactor and the enzyme were $1.9 \times 10^{-7}$ M and $7.5 \times 10^{-6}$ M (protomer), respectively. The concentration of the nucleic acid was $6.5 \times 10^{-5}$ M (oligomer). For the sake of companson, the time course of ATP hydrolysis by a single, noninteracting site of the DnaB helicase hexamer in the absence of the ssDNA 20-mer is included in the panel, at the same cofactor and enzyme concentrations (□). The solid line is the nonlinear least-squares fit of the double-exponential function (eq 1) to the experimental curve. (b) Dependence of the reciprocal of the relaxation time, $1/\tau_1$, for ATP hydrolysis by the single, noninteracting site of the DnaB helicase in buffer T4, in the presence of $dC(pC)_{19}$, on the total concentration of the enzyme (protomer). The solid line is a numerical, nonlinear least-squares fit of the experimental data to the three-step sequential mechanism, defined by Scheme 1. (c) Dependence of the reciprocal of the relaxation time, $1/\tau_2$, for ATP hydrolysis by the single, noninteracting site of the DnaB helicase in buffer T4, in the presence of $dC(pC)_{19}$, on the total concentration of the enzyme (protomer). The solid line is a numerical, nonlinear least-squares fit of the experimental data to the three-step sequential mechanism, defined by Scheme 1. The error bars in panels b and c are standard deviations determined in three normalized total and individual relaxation amplitudes, $A_T$ (▲), $A_1$ (■), and $A_2$ (□), of ATP hydrolysis by a single, noninteracting site of the DnaB helicase in buffer T4, in the presence of $dC(pC)_{19}$, on the total concentration of the enzyme (protomer). The solid lines are nonlinear least-squares fits according to the three-step sequential mechanism of ATP hydrolysis in the noninteracting site of the helicase, described by Scheme 1. The rate constants, obtained from the fits of the relaxation times and the amplitudes, are included in Table 1.

Scheme 1

$$\text{helicase} + \text{NTP} \underset{k_{-1}}{\overset{k_1}{\rightleftarrows}} \text{H-NTP} \underset{k_{-2}}{\overset{k_2}{\rightleftarrows}} (\text{H-NDP}\cdot\text{P}_\text{i})_1 \underset{k_{-3}}{\overset{k_3}{\rightleftarrows}} (\text{H-NDP}\cdot\text{P}_\text{i})_2$$

to $dA(pA)_{19}$ (Table 1). Because the chemical step is too fast to be accessed in the rapid quench-flow experiment (see above), only the minimum values of both $k_2$ and $k_{-2}$ for $dA(pA)_{19}$ could be determined. Thus, the presence of the homoadenine 20-mer increases the rate of hydrolysis in both directions by a factor of at least ~11, as compared to the free enzyme. On the other hand, the presence of $dC(pC)_{19}$ and $dT(pT)_{19}$ decreases the forward rate constant, $k_2$, by factors of ~6 and ~3, respectively. Moreover, a much less pronounced effect of both cytidine and thymine ssDNA oligomers is observed on the backward rate constant of the hydrolysis step, $k_{-2}$, as compared to the free enzyme. Finally, the presence of all examined ssDNA oligomers predominantly affects the backward rate constant, $k_{-3}$, of the slow conformational transition [$(\text{H-ADP}\cdot\text{P}_\text{i})_1 \leftrightarrow (\text{H-ADP}\cdot\text{P}_\text{i})_2$] (Scheme 1), Surprisingly, the presence of $dC(pC)_{19}$ increases the rate constants of GTP hydrolysis and strongly increases the forward rate constant, $k_3$, of the slow conformational transition, making the $(\text{H-GDP}\cdot\text{P}_\text{i})_1 \leftrightarrow (\text{H-GDP}\cdot\text{P}_\text{i})_2$ step the most energetically favorable among the examined systems (see Discussion).

*Effect of Different ssDNA Homo-Oligomers on the CTP Hydrolysis Reaction Catalyzed by the DnaB Helicase.* A rapid quench-flow kinetic curve of [α-$^{32}$P]CTP hydrolysis after $1.9 \times 10^{-7}$ M CTP had been mixed with the DnaB helicase ($7 \times 10^{-6}$ M) (protomer) and the ssDNA oligomer, $dA(pA)_{19}$, [$6.5 \times 10^{-5}$ M (oligomer)] (final concentrations) in buffer T4 is shown in Figure 7a. The kinetic curve, obtained in the absence of the ssDNA 20-mer, is also included in Figure 7a. As observed in the case of ATP, the presence of $dA(pA)_{19}$ strongly increases the rate of product formation, particularly, in the hydrolysis step. The kinetic curve in Figure 7a becomes clearly biphasic. Nevertheless, the total amplitude of the normalized product formation, $A_T$, does not reach a value of 1. Moreover, there is no a time lag in

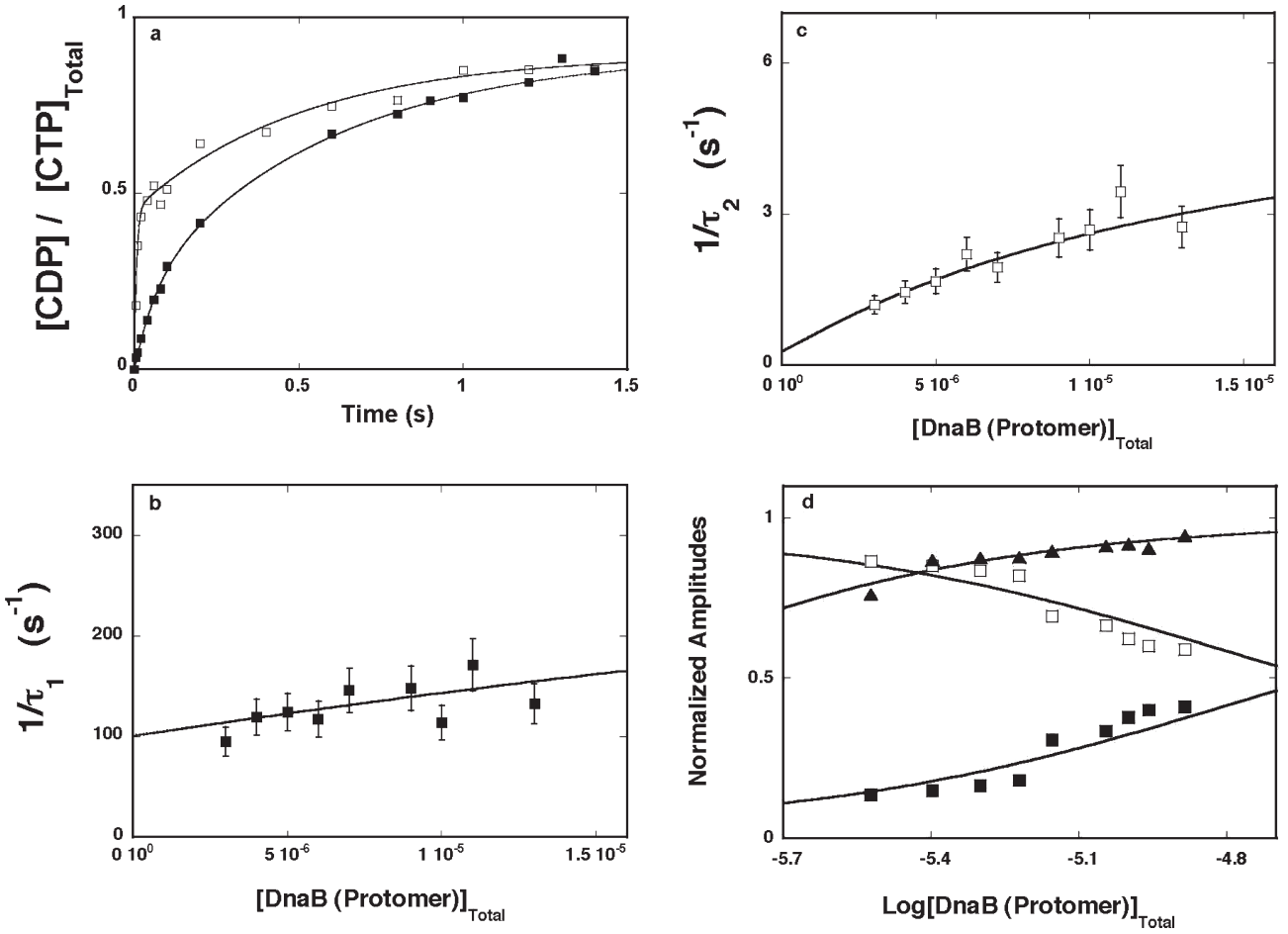


FIGURE 7: (a) Time course of CTP hydrolysis by a single, noninteracting site of the DnaB helicase hexamer in the presence of the ssDNA 20-mer, $dA(pA)_{19}$ (□), in single-turnover experiments, in buffer T4. The produced CDP is shown as a fraction of the total concentration of CTP in the sample. The concentrations of the cofactor and the enzyme were $1.9 \times 10^{-7}$ M and $7.5 \times 10^{-6}$ M (protomer), respectively. The concentration of the nucleic acid was $6.5 \times 10^{-5}$ M (oligomer). For the sake of comparison, the time course of CTP hydrolysis by a single, noninteracting site of the DnaB belicase hexamer, in the absence of the ssDNA 20-mer, is included in panel a, at the same cofactor and enzyme concentrations (■). The solid line is the nonlinear least-squares fit of the double-exponential function (eq 1) to the experimental curve. (b) Dependence of the reciprocal of the relaxation time, $1/\tau_1$, for CTP hydrolysis by the single, noninteracting site of the DnaB helicase in buffer T4, in the presence of $dA(pA)_{19}$, on the total concentration of the enzyme (protomer). The solid line is a numerical, nonlinear, least-squares fit of the experimental data to the three-step sequential mechanism, defined by Scheme 1. (c) Dependence of the reciprocal of the relaxation time, $1/\tau_2$, for CIP hydrolysis by the single, noninteracting site of the DnaB helicase in buffer T4, in the presence of $dA(pA)_{19}$, on the total concentration of the enzyme (protomer). The solid line is a numerical, nonlinear, least-squares fit of the experimental data to the three-step sequential mechanism, defined by Scheme 1. The error bars in panels b and c are standard deviations determined in three or four independent experiments. (d) Dependence of the normalized, total, and individual relaxation amplitudes, $A_T$ (▲), $A_1$ (■), and $A_2$ (□), respectively, of CTP hydrolysis by a single, noninteracting site of the DnaB helicase in buffer T4, in the presence of $dA(pA)_{19}$, on the total concentration of the enzyme (protomer). The solid lines are nonlinear, least-squares fits according to the three-step sequential mechanism of CTP hydrolysis in the noninteracting site of the helicase, described by Scheme 1. The rate constants, obtained from the fits of the relaxation times and the amplitudes, are included in Table 1.

the examined product formation. The solid line in Figure 7a is a nonlinear least-squares fit of the experimental curve, using eq 1 with a double-exponential function, to extract the relaxation times, $1/\tau_1$ and $1/\tau_2$, and amplitudes, $A_1$ and $A_2$, of the process. The dependencies of $1/\tau_1$ and $1/\tau_2$ on the DnaB helicase concentration (protomer) are shown in panels b and c of Figure 7, respectively. The dependencies of the normalized total, $A_T$, and the corresponding individual amplitudes, $A_1$ and $A_2$, on the logarithm of the total DnaB protein concentration (protomer) are shown in Figure 7d. The value of $1/\tau_1$ changes linearly with $[DnaB]_T$, while $1/\tau_2$ shows a hyperbolic dependence upon the enzyme concentration. However, the absence of the time lag and the behavior of the amplitudes with respect to $[DnaB]_T$ indicate that two products containing CDP are observed (*31*). The solid lines in panels b−d of Figure 7 are nonlinear least-squares fits of the relaxation times and amplitudes according to the mechanism defined by Scheme 1. Analogous experiments have been performed with different ssDNA homo-oligomers. The obtained rate and equilibrium constants of the CTP hydrolysis, for all examined nucleic acids, are included in Table 1.

As opposed to those of the purine cofactors, ATP and GTP, the value of the partial equilibrium constant, $K_1$, is only slightly increased, as compared to the same parameter obtained for the free enzyme, even in the presence of $dA(pA)_{19}$ (see Discussion). However, the partial equilibrium constants, $K_2$ and $K_3$, are decreased and increased, respectively, similar to the effect exerted by the nucleic acid in the case of the purine cofactors (Table 1). Also, similar to the purine cofactors, the major difference among the ssDNA 20-mers is in their effect on the rate of ATP hydrolysis, as compared to the adenine 20-mer (Table 1). In the presence of $dA(pA)_{19}$, the values of $k_2$ and $k_{-2}$, characterizing the chemical step, are increased by factors of ~5 and ~9, respectively, as compared to the same parameters obtained in the absence of the nucleic acid. Nevertheless, the value of $k_2$ is

still significantly lower than the minimum value of the same parameter obtained for ATP (Table 1). On the other hand, $k_2$ is diminished by a factor of only ~1.4 in the case of dC(pC)$_{19}$ and increased by a factor of only ~1.5 in the presence of dT(pT)$_{19}$, as compared to the free helicase, making the forward rate of CTP hydrolysis similar to the rate observed for ATP, in the presence of the same ssDNA oligomer. The presence of all examined ssDNA oligomers increases the rate constant, $k_3$, and only slightly affects the backward rate constant, $k_{-3}$, of the slow conformational transition [(H-CDP·P$_i$)$_1$ ↔ (H-CDP·P$_i$)$_2$] (Scheme 1) (see Discussion).

*Allosteric Effect of the Strong and Weak DNA-Binding Subsites on the Kinetics of the NTP Hydrolysis by the DnaB Helicase*. As mentioned above, the DnaB helicase binds the ssDNA in a strictly single orientation with respect to the sugar−phosphate backbone of the nucleic acid, with only one subunit engaged in the interactions with the nucleic acid in the stationary complex (*24*, *25*). Moreover, the total DNA-binding site, which occludes ~20 nucleotides of the nucleic acid, has heterogeneous structure and is built of two DNA-binding subsites (*24*, *25*). The strong DNA-binding subsite occludes ~10 nucleotides at the 5′ end of the bound ssDNA, while the weak DNA-binding subsite occludes ~10 nucleotides at the 3′ end of the bound nucleic acid. The DnaB−ssDNA complex is schematically shown in Figure 8. The extent to which these DNA-binding subsites are interdependent is unknown. We first addressed this issue using fluorescent etheno derivatives of the ssDNA oligomers, whose emission is greatly sensitive to the structure of the nucleic acid and much less sensitive to the properties of the environment (*34*−*37*) (see Discussion).

The fluorescence titration curves of the ssDNA 20-mers, dεA(pεA)$_{19}$, dεA(pεA)$_9$(dT)$_{10}$, and dT(pT)$_9$(dεA)$_{10}$, in buffer T4, containing 1 mM AMP-PNP, are shown in Figure 9. The solid lines in Figure 9 are nonlinear least-squares fits of the experimental curves, using a single-site binding isotherm

$$\Delta F_{obs} = \Delta F_{max}\left(\frac{K[P]_F}{1 + K[P]_F}\right) \quad (3)$$

where $K$ is the macroscopic binding constant, $\Delta F_{max}$ is the maximum observed fluorescence increase, and $[P]_F$ is the free concentration of the DnaB protein (*41*).

When both DNA-binding subsites are filled with ethenoadenosine nucleotides, as is the case with dεA(pεA)$_{19}$, the binding of the oligomer is accompanied by a large, ~260%, increase in nucleic acid fluorescence. However, when only the strong DNA-binding subsite is engaged in interactions with the ethenoadenosines, as is the case with dεA(pεA)$_9$(dT)$_{10}$, the relative increase in nucleic acid fluorescence is dramatically lower, reaching only ~85%. More surprising is the fact that engagement of only the weak DNA-binding site in interactions with the ethenoadenosines, in the complex with dT(pT)$_9$(dεA)$_{10}$, induces the $\Delta F_{max}$ value of ~100%, which is larger than when the strong DNA-binding site interacts with the fluorescent nucleotides (Figure 9). The highest and lowest affinities are observed for dεA(pεA)$_{19}$ and dεA(pεA)$_9$(dT)$_{10}$, respectively. This is also surprising, as the affinity of the ssDNA is largely, if not exclusively, determined by the interactions with the strong DNA-binding subsite, which in both cases contains the same nucleotides (*25*). Such behavior provides the first structural and functional indication that the interactions in the strong and weak DNA-binding subsites, as reflected by the etheno derivative fluorescence

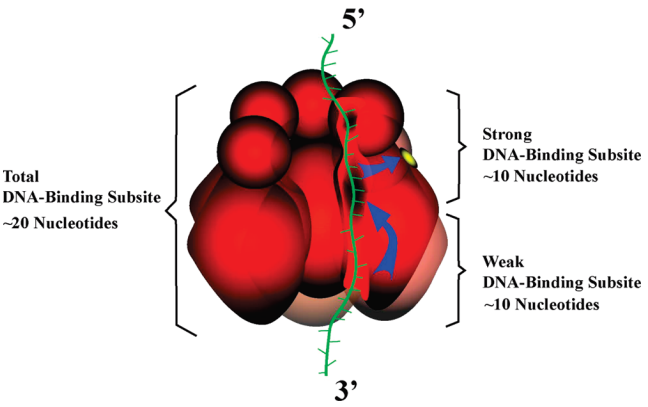


FIGURE 8: Schematic structure of the DnaB hexamer−ssDNA complex based on thermodynamics, fluorescence energy transfer studies, and biochemical data (*24*, *25*, *27*, *58*). Each DnaB subunit is built of a small ~12 kDa domain and a large ~33 kDa domain. The total ssDNA-binding site occludes ~20 nucleotides of the DNA. The strong DNA-binding subsite is located in the vicinity of the 12 kDa domain and occludes ~10 nucleotides at the 5′ end of the bound nucleic acid. The weak DNA-binding subsite occludes a similar number of ~10 nucleotides and is located in the 33 kDa domain of the helicase. The yellow oval indicates the location of the NTP-binding site. The arrows indicate the functional directions of the allosteric effects of the nucleic acid on the NTPase site of the enzyme. The strong DNA-binding subsite directly interacts with the NTPase site. The effect of the weak DNA-binding subsite is indirect, through its modulation of the DNA structure in the strong subsite.

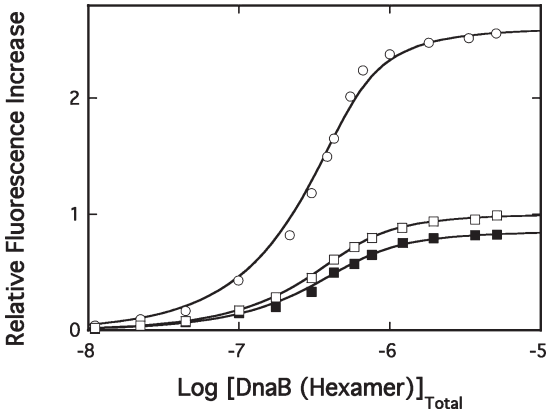


FIGURE 9: Fluorescence titrations ($\lambda_{ex}$ = 325 nm; $\lambda_{em}$ = 410 nm) of the etheno derivative of the ssDNA 20-mers, dεA(pεA)$_{19}$ (○), dεA(pεA)$_9$(pT)$_{10}$ (■), and dT(pT)$_9$(pεA)$_{10}$ (□), with the DnaB helicase in buffer T4 (pH 8.1 and 20 °C). The concentration of all ssDNA oligomers was $4.5 \times 10^{-7}$ M (oligomer). The solid lines are nonlinear, least-squares fits of the titration curves to a single-binding site isotherm (eq 3) with two fitting parameters: $K = 1.5 \times 10^7$ M$^{-1}$, and $\Delta F_{max} = 2.6$ (○); $K = 8 \times 10^6$ M$^{-1}$, and $\Delta F_{max} = 0.85$ (■); $K = 1.1 \times 10^7$ M$^{-1}$, and $\Delta F_{max} = 1.0$ (□).

and affinities of the selected ssDNA 20-mers, are affected by the character of interactions occurring in the neighboring subsite (see Discussion).

The dramatic difference between the effect of the adenine ssDNA 20-mer, dA(pA)$_{19}$, and the effect of the cytidine oligomer, dC(pC)$_{19}$, on NTP hydrolysis (Table 1) allows us to further address the role of the two structural and functional elements of the total DNA-binding site of the DnaB helicase, the strong and weak DNA-binding subsites, in the enzymatic reaction. To examine the effect of both subsites on NTP hydrolysis, we used two different ssDNA 20-mers, analogous to the oligomers used in the binding studies discussed above (Figure 9). The first oligomer, dA(pA)$_9$(pC)$_{10}$, has 10 adenosine nucleotides at the 5′ end, and

the 10 remaining nucleotides are cytidines. The second oligomer, $dC(pC)_9(pA)_{10}$, has 10 cytidine nucleotides at the 5′ end, and the 10 remaining nucleotides are adenosines. Thus, when bound, the first oligomer has 10 adenosines in the strong DNA-binding subsite and the second 20-mer has 10 cytidines in the strong subsite (*25*). In these experiments, we used CTP, because even in the presence of $dA(pA)_{19}$, the two observed relaxation processes are accessible in the time range of the rapid quench-flow measurements (Figure 7a) (see above).

The rapid quench-flow kinetic curves of [α-$^{32}$P]CTP hydrolysis after $1.9 \times 10^{-7}$ M CTP had been mixed with the DnaB helicase ($7 \times 10^{-6}$ M) (protomer) and the ssDNA oligomer, $dA(pA)_9(pC)_{10}$ or $dC(pC)_9(pA)_{10}$ [$6.5 \times 10^{-5}$ M (oligomer)] (final concentrations), are shown in Figure 10. The kinetic curve obtained in the presence of $dA(pA)_{19}$ is also included in Figure 10. The effect of $dA(pA)_9(pC)_{10}$ on the observed product formation is dramatic. The rate of the hydrolysis step, which is clearly observable in the presence of $dA(pA)_{19}$, is now beyond the time resolution of the rapid quench-flow technique. However, the amplitude of the fast step is lower than that observed in the presence of homoadenine 20-mer, indicating that the equilibrium of the hydrolysis step is shifted toward CTP (see above). The presence of the ssDNA 20-mer, $dC(pC)_9(pA)_{10}$, also increases the rate of the hydrolytic step, as compared to the rates observed for the enzyme in the absence of the nucleic acid, although the effect is significantly less pronounced than that observed for $dA(pA)_9(pC)_{10}$ and the entire relaxation process is within the time range of the rapid quench-flow measurement. The solid lines in Figure 10 are nonlinear least-squares fits of the experimental curve using eq 1 with a single-exponential function for $dA(pA)_9(pC)_{10}$ data, which provides $1/\tau_2$ and $A_2$, and a double-exponential function for the $dC(pC)_9(pA)_{10}$ kinetic curve, which provides $1/\tau_1$, $1/\tau_2$, $A_1$, and $A_2$, characterizing both kinetic relaxation processes.

For $dA(pA)_9(pC)_{10}$, the dependence of $1/\tau_2$ on the DnaB helicase concentration (protomer) is shown in Figure 11a. The hyperbolic shape of the plot indicates that it described an intramolecular transition (*31*, *39*, *41*−*43*). The dependences of the normalized total, $A_T$, and individual amplitudes, $A_1$ and $A_2$, of the observed relaxation processes upon DnaB concentration (protomer) are shown in Figure 11b. The amplitude of the hydrolysis step has been obtained as the difference ($A_1 = A_T - A_2$) (see above) (*31*). The functional dependence of amplitudes on the enzyme concentration indicates that the simplest kinetic mechanism of the examined reaction is described by Scheme 1. Nevertheless, with only a single relaxation time and three amplitudes available from the experiments, we can directly determine only the product, $K_1K_2$, for the two fast steps. However, as discussed above, the amplitudes of the observed fast step are similar for $dA(pA)_9(pC)_{10}$ and $dC(pC)_9(pA)_{10}$, indicating very similar values of $K_2$ (Figure 10). Taking the same value of $K_2$ for $dA(pA)_9(pC)_{10}$ as the value of the corresponding parameter obtained for $dC(pC)_9(pA)_{10}$ allows us to estimate the value of $K_1$ for $dA(pA)_9(pC)_{10}$. The solid lines in panels a and b of Figure 11 are nonlinear least-squares fits of the relaxation times and amplitudes according to the mechanism defined by Scheme 1. The obtained rate and equilibrium constants are included in Table 1.

In the case of $dC(pC)_9(pA)_{10}$, the dependencies of $1/\tau_1$ and $1/\tau_2$ on the DnaB helicase concentration (protomer) are shown in panels a and b of Figure 12, respectively. The dependencies of the normalized total $A_T$ and the corresponding individual amplitudes, $A_1$ and $A_2$, on DnaB concentration are shown in Figure 12c. The value of $1/\tau_1$ changes linearly with enzyme concentration, while $1/\tau_2$ shows a hyperbolic dependence on the enzyme concentration. However, the absence of the time lag and the behavior of the amplitudes with respect the DnaB concentration indicate that two products containing CDP are observed (*31*). The solid lines in panels a−c of Figure 12 are nonlinear least-squares fits of the relaxation times and amplitudes, according to the mechanism defined by Scheme 1. The obtained rate and equilibrium constants of CTP hydrolysis for $dA(pA)_9(pC)_{10}$ and $dC(pC)_9(pA)_{10}$ are included in Table 1.

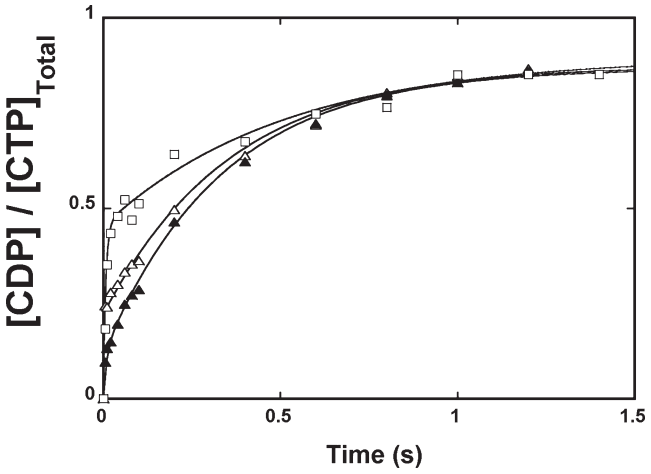


FIGURE 10: Time course of CTP hydrolysis by a single, noninteracting site of the DnaB helicase hexamer in the presence of the ssDNA 20-mers $dC(pC)_9(pA)_{10}$ (▲), $dA(pA)_9(pC)_{10}$ (△), and $dA(pA)_{19}$ (□), in single-turnover experiments, in buffer T4. The produced CDP is shown as a fraction of the total concentration of the CTP in the sample. The concentrations of the cofactor and the enzyme were $1.9 \times 10^{-7}$ M and $7.5 \times 10^{-6}$ M (protomer), respectively. The concentrations of all nucleic acids were $6.5 \times 10^{-5}$ M (oligomer). The solid lines are the nonlinear, least-squares fits of the double-exponential function (eq 1) to the experimental kinetic curves (details in the text).

The values of the partial equilibrium constant, $K_1$, are, within experimental accuracy, the same as those obtained for the free enzyme, i.e., in the absence of $dA(pA)_9(pC)_{10}$ and $dC(pC)_9(pA)_{10}$. The partial equilibrium constants, $K_2$, which describe the chemical, hydrolysis step [H-CTP ↔ (H-CDP·$P_i$)$_1$], are decreased as compared to the same parameter in the absence of the DNA, or in the presence of the homo-oligomers. However, the values of $K_3$ are significantly higher than those observed in the presence of the homo-oligomers, making the transition of the enzyme−product complex, following the chemical step, as energetically favorable as those observed for the GTP cofactor in the presence of the ssDNA homo-oligomers (Table 1). However, the presence of different ssDNAs in the strong and weak DNA-binding sites dramatically affects the rate constants of CTP hydrolysis (Table 1). In the case of $dA(pA)_9(pC)_{10}$, only the minimum values of $k_2$ and $k_{-2}$ could be determined. The presence of adenines in the strong DNA-binding subsite and cytidines in the weak subsite increases the forward rate constant of hydrolysis, $k_2$, by factors of at least ~20 and ~4, as compared to the free enzyme and the enzyme associated with $dA(pA)_{19}$, respectively. An even more dramatic effect is observed on $k_{-2}$, where the corresponding factors are ~100 and ~10, respectively. On the other hand, the presence of cytidines in the strong DNA-binding subsite and adenines in the weak subsite increases the forward rate constant of hydrolysis, $k_2$, by a factor of only ~2 and decreases $k_2$ by a factor of ~2, as compared to those of the free enzyme and the enzyme associated with $dA(pA)_{19}$, respectively.

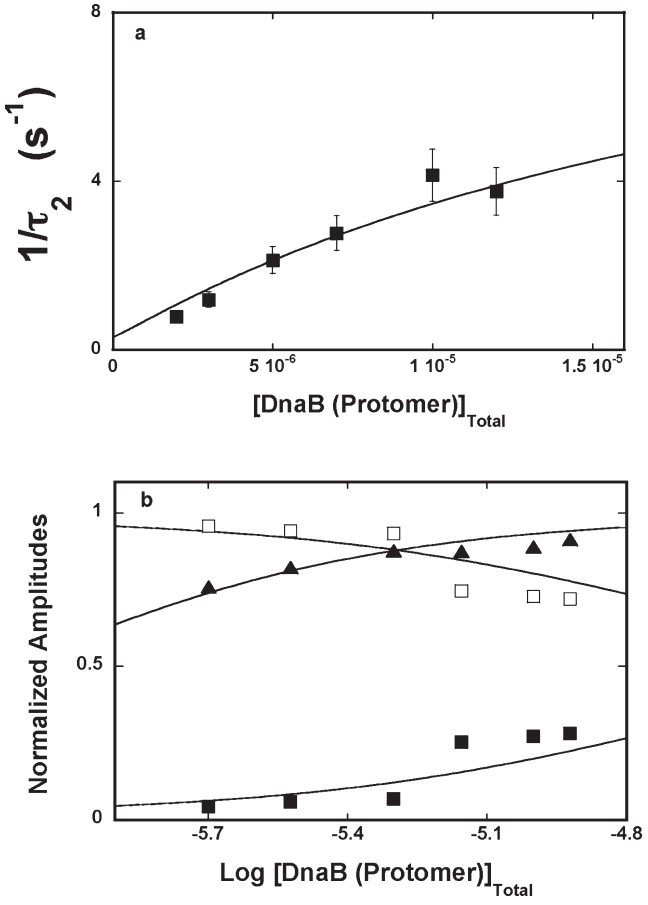


FIGURE 11: (a) Dependence of the reciprocal of the relaxation time, $1/\tau_2$, for CTP hydrolysis by the single, noninteracting site of the DnaB helicase, in the presence of $dA(pA)_9(pC)_{10}$, on the total concentration of the enzyme (protomer). The solid line is a nonlinear, least-squares fit of the experimental data to the three-step sequential mechanism, defined by Scheme 1. (b) Dependence of the normalized, total, and individual relaxation amplitudes, $A_T$ (▲), $A_1$ (■), and $A_2$ (□), of CTP hydrolysis by a single, noninteracting site of the DnaB helicase, in the presence of $dA(pA)_9(pC)_{10}$, on the concentration of the enzyme (protomer). The solid lines are nonlinear, least-squares fits according to the three-step sequential mechanism of CTP hydrolysis, described by Scheme 1. The rate constants, obtained from the fits of the relaxation times and the amplitudes, are included in Table 1.

The backward rate constant of the hydrolysis step, $k_{-2}$, is, within experimental accuracy, the same as that determined for $dA(pA)_{19}$ (Table 1). The presence of both mixed ssDNA oligomers affects the slow conformational transition $[(H\text{-}ADP\cdot P_i)_1 \leftrightarrow (H\text{-}ADP\cdot P_i)_2]$ (Scheme 1) through the increased values of the forward rate constant, $k_3$, which becomes similar to the value observed for homo-oligomer $dC(pC)_{19}$ (see Discussion).

## DISCUSSION

*The Multiple-Step Kinetic Mechanism of NTP Binding and Hydrolysis by a Single, Noninteracting Site on the DnaB Helicase Is Independent of the Type of Base of the Nucleotide Cofactor*. Binding and hydrolysis of NTP cofactors by the DnaB helicase, prior to association with the nucleic acid, are fundamental processes that induce and modulate the high-affinity conformation of the enzyme for the single-stranded nucleic acid (*1*−*5*). Moreover, the efficiency of the dsDNA unwinding and the rate of mechanical translocation along the nucleic acid lattice are intimately dependent upon the NTP hydrolysis rate, which provides energy for these two activities.

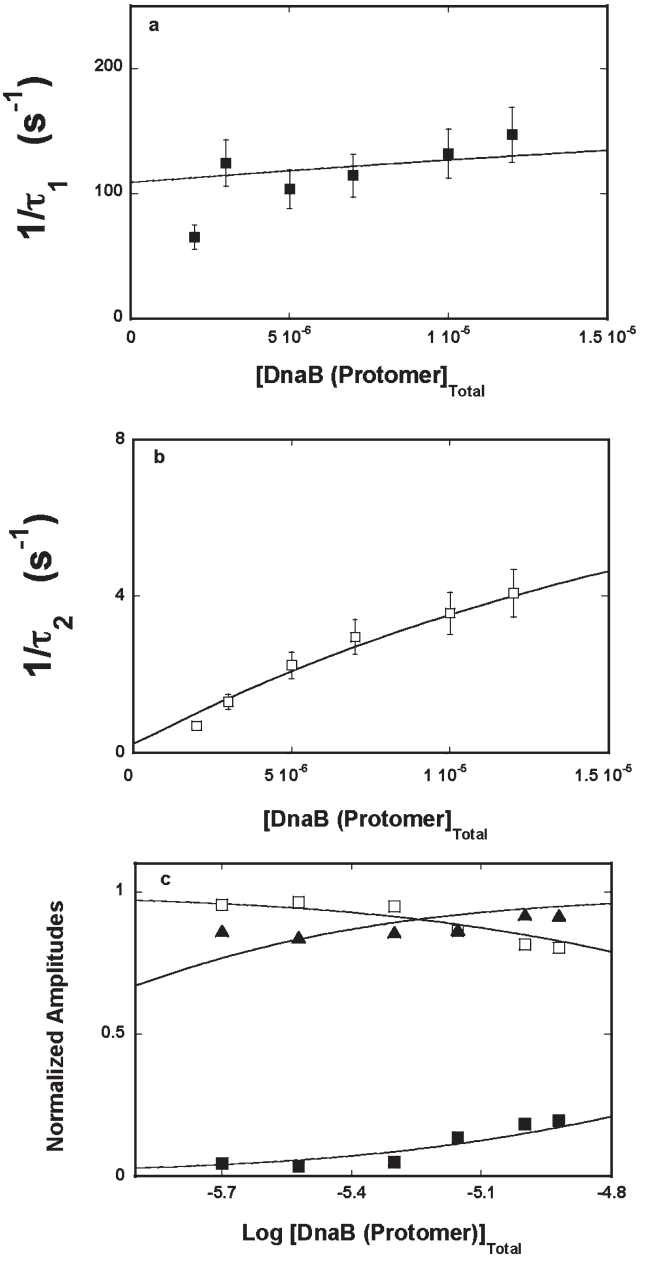


FIGURE 12: (a) Dependence of the reciprocal of the relaxation time, $1/\tau_1$, for CTP hydrolysis by the single, noninteracting site of the DnaB helicase in buffer T4, in the presence of $dC(pC)_9(pA)_{10}$, on the total concentration of the enzyme (protomer). The solid line is a nonlinear, least-squares fit of the experimental data to the three-step sequential mechanism, defined by Scheme 1. (b) Dependence of the reciprocal of the relaxation time, $1/\tau_2$, for CTP hydrolysis by the single, noninteracting site of the DnaB helicase in buffer T4, in the presence of, $dC(pC)_9(pA)_{10}$, on the total concentration of the enzyme (protomer). The solid line is a nonlinear, least-squares fit of the experimental data to the three-step sequential mechanism, defined by Scheme 1. The error bars in panels a and b are standard deviations determined from three or four independent experiments. (c) Dependence of the normalized, total, and individual relaxation amplitudes, $A_T$ (▲), $A_1$ (■), and $A_2$ (□), of CTP hydrolysis by a single, noninteracting site of the DnaB helicase, in buffer T4, in the presence of $dC(pC)_9(pA)_{10}$, on the total concentration of the enzyme (protomer). The solid lines are nonlinear, least-squares fits according to the three-step sequential mechanism of CTP hydrolysis, described by Scheme 1. The rate constants, obtained from the fits of the relaxation times and the amplitude, are included in Table 1.

Early steady-state analyses have shown that the DnaB helicase can bind and hydrolyze NTPs, in a manner independent of the type of the base of the cofactor, but only in the presence of

the DNA (*11*, *12*). The first quantitative indication about the differences in interactions between the free DnaB helicase and different nucleotide cofactors came from the thermodynamic studies, which indicated strong, ground-state preference of the helicase for the purine nucleotide, ATP and GTP (*27*−*29*). Nevertheless, the single-turnover experiments, discussed in this work, provide strong evidence that the major aspects of the kinetic mechanism of the hydrolysis are the same, for all examined nucleotide cofactors (*31*).

The application of the relaxation kinetic approach in our studies was introduced on the basis of the fact that the total amplitude of the single-turnover kinetic curves of NTP binding and hydrolysis by the DnaB helicase never reaches 100% of the available total cofactor concentration. If the kinetic mechanism in the enzyme active site included an irreversible step, then ~100% hydrolysis of each NTP would have been observed. The simplest explanation of these experimental facts is that all steps, in the time range of the single-turnover experiments, can be treated as reversible transitions. Moreover, there is no time lag in any of the measured kinetic curves, even at the lowest enzyme concentration applied. Such behavior results from the observation of at least two intermediates containing the observed product of the reaction, NDP (*31*). If only the final species of the reaction mixture containing NDP were monitored, then the time lag in the NDP formation would be clearly observed in the studied enzyme concentration ranges (*31*). Consequently, the double-exponential function (eq 1) is required to adequately represent the binding and hydrolysis reaction. Thus, single-turnover experiments provide strong evidence that the mechanism of binding and hydrolysis of pyrimidine, CTP, and purine, ATP and GTP, cofactors, by a single, noninteracting site on the DnaB helicase, is a minimum three-step sequential process, described by Scheme 1. In other words, the kinetic mechanism of NTP hydrolysis by the DnaB helicase is independent of the type of the base of the nucleotide cofactor.

*The Sequential Mechanism of the NTP Binding and Hydrolysis Excludes the Pre-Equilibrium Conformational Transition of the DnaB Helicase*. The sequential nature of the kinetic mechanism of NTP binding and hydrolysis contains additional information. It indicates that the formation of different intermediates, or conformational states of the helicase, occurs as a response to the formation of the enzyme−nucleotide complex and undergoing catalysis and is independent of the type of the base of the nucleotide cofactor. In other words, the observed differences in the ground-state affinities between the purine and pyrimidine cofactors are not a result of recognizing different states of the enzyme by a different type of cofactor prior to binding. In this context, the single-turnover data are in excellent agreement with the results of the stopped-flow studies on the formation of the ground states of the helicase−nucleotide complexes, which also occur through the sequential multiple-state mechanism (*30*). Previous sedimentation studies have shown that binding of nucleotide cofactors to the *E. coli* DnaB and plasmid RSF1010 RepA hexamers induces large global conformational changes in the hexamer (*48*). Moreover, electron microscopy results showed the presence of different conformational states of the DnaB helicase, even prior to the nucleotide binding (*49*, *50*). However, the sequential nature of the dynamics of different nucleotide cofactors binding and hydrolysis by the DnaB helicase, as well as previous stopped-flow studies, indicates that the ground-state affinity of these different states for the cofactors must be very similar, and once nucleotide binding has occurred, they undergo transitions to the same kinetic intermediates (see below).

*The Chemical NTP Hydrolysis Step by a Single, Noninteracting Site on the DnaB Helicase Is Significantly Faster for the Purine Nucleotide Cofactors, ATP and GTP, Than for the Pyrimidine Cofactor, CTP*. The NTP hydrolysis step [H-NTP ↔ (H-NDP·$P_i$)$_1$] is much faster in the case of the purine cofactors than in the case of CTP (Figure 2). While the values of $k_2$ are ~258 and ~220 $s^{-1}$ for ATP and GTP, respectively, it is only ~83 $s^{-1}$ for CTP (Table 1). Analogously, the values of the backward rate constant of the hydrolysis step, $k_{-2}$, are ~52 and 21 $s^{-1}$ for ATP and GTP, respectively, and only ~9.9 $s^{-1}$ in the case of CTP. Thus, although the kinetic mechanism of NTP binding and hydrolysis by the single, noninteracting site on the DnaB helicase is independent of the type of the base of NTP cofactors, the purine and pyrimidine nucleotides strongly differ in the dynamics of the chemical step of the reaction. Our recent studies on the analogous RepA hexameric helicase indicate that the binding of the first and second nucleotide cofactor molecules to the helicase induces large global conformational changes in the enzyme (*48*). Moreover, the nucleoside triphosphate induces a conformational state that has a much higher affinity for the ssDNA and a larger site size of the protein−nucleic acid complex than the diphosphate cofactor. Therefore, the dynamics of these conformational changes will depend on the dynamics of the NTP hydrolysis step. The kinetic data indicate that the type of nucleotide controls the rate of the global conformational changes of the helicase, which will be significantly slower in the presence of pyrimidine than purine cofactors. This will happen prior to the binding to the nucleic acid and also in the complex with the DNA (see below).

*The Nature of Intermediates of the Purine Cofactor, ATP, in the Binding and Hydrolysis Reaction Is Different from the Nature of the Analogous Intermediates of the Pyrimidine Cofactor, CTP*. Interestingly, the values of the partial equilibrium constants, $K_1$, $K_2$, and $K_3$, characterizing the internal energetics of different intermediates, formed in the NTP binding and hydrolysis by the noninteracting site of the DnaB helicase, are similar, although not identical, for both purine, ATP and GTP, and pyrimidine cofactors, CTP (Table 1). Nevertheless, dramatic differences in the changes in the thermodynamic function, $\Delta H$ and $\Delta S$, accompanying the formation of different intermediates in the ATP versus CTP hydrolysis reaction indicate that beneath the similar values of the partial equilibrium constants, intermediates of different natures are formed (Table 2). The observed sequence of the reaction steps [H + NTP ↔ H-NTP ↔ (H-NDP·$P_i$)$_1$ ↔ (H-NDP·$P_i$)$_2$] is exothermic → endothermic → endothermic for ATP and endothermic → exothermic → exothermic for CTP. The values of $\Delta H_1$ for both cofactors are much larger than expected for a simple, diffusion-controlled biomolecular association (*51*). The data indicate that the observed binding step must include an additional fast conformational transition(s).

Large negative values of $\Delta H_1$ (approximately −18.4 kcal/mol) and $\Delta S_1$ (approximately −44 cal $mol^{-1}$ $°C^{-1}$), in the case of ATP, strongly suggest that the observed structural changes in the H-NTP intermediate extend beyond the local environment of the NTP binding site. Because binding of nucleotide cofactors is usually accompanied by the release of water molecules, which would contribute to a positive entropy change, the data indicate that the purine cofactor forms several short-range bonds in the binding site contributing to negative enthalpy change (*52*, *53*).

The resulting strong immobilization of ATP in the H-ATP intermediate would compensate for the positive entropy changes due to the release of water molecules. In the case of CTP, the binding step is energetically unfavorable and driven by a large and positive $\Delta S_1$ of $\approx$52 cal mol$^{-1}$ °C$^{-1}$, strongly suggesting that the pyrimidine cofactor is much less immobilized in the H-CTP intermediate and the solvent release from the complex dominates the binding step. The chemical hydrolysis step is energetically unfavorable and entropy-driven for ATP, suggesting that some of the immobilizing interactions in the H-ATP complex are released in the (H-ADP·$P_i$)$_1$ intermediate. The large entropy change and small but unfavorable enthalpy change in the (H-ADP·$P_i$)$_1$ ↔ (H-ADP·$P_i$)$_2$ transition suggest that the process of releasing the cofactor from the initial immobilization continues through the third step of the reaction. On the other hand, the pyrimidine cofactor becomes more immobilized in the binding site through the course of the reaction, as the individual steps are characterized by only modest negative changes in enthalpy and positive changes in entropy (Table 2). Notice, in spite of the very different natures of the intermediates, the entire three-step process of binding and hydrolysis is, for both the purine and the pyrimidine cofactor, an entropy-driven reaction, strongly suggesting that both types of cofactors approach a similar exit state at the end of the reaction.

*The Effect of the ssDNA on the Kinetics of NTP Hydrolysis by the DnaB Helicase Depends on the Type of Nucleotide Cofactor and the Base Composition of the Nucleic Acid and Is Centered at the Chemical Hydrolysis Step*. A strong stimulatory effect of the nucleic acid on the NTP hydrolysis by the DnaB helicase has been previously observed (*11*, *12*). However, the data obtained in this work show that the effect is much more complex than a simple activation. The difference between the effect of dA(pA)$_{19}$ and dC(pC)$_{19}$ and dT(pT)$_{19}$ on the NTP hydrolysis step [H-NTP ↔ (H-NDP·$P_i$)$_1$] catalyzed by the DnaB helicase is striking. Although it is observed for all studied cofactors, it is particularly pronounced for the purine cofactors, ATP and GTP. Both rate constants, $k_2$ and $k_{-2}$, are increased by at least 1 order of magnitude in the presence of the adenine homo-oligomer, as compared to the free enzyme (Table 1). In fact, dC(pC)$_{19}$ and dT(pT)$_{19}$ make the forward rate constant, $k_2$, of the hydrolysis step profoundly lower than that observed for the free enzyme. The specific effect of dA(pA)$_{19}$ on the rate of hydrolysis is also clearly observed for CTP. Nevertheless, it is much more modest than that observed for the purine cofactors.

There are two fundamental functional aspects of these results. First, the efficiency of the dsDNA unwinding and mechanical translocation of the enzyme depends on the rate of NTP hydrolysis, which provides the necessary free energy (*32*, *33*, *44*). The obtained data indicate that the DnaB helicase will have different rates of dsDNA unwinding and mechanical translocation, depending on the sequence of the replication fork arm, to which it is bound. In fact, we have already observed that the rate of dsDNA unwinding on the nucleic acid containing 50% adenosine nucleotides is 1 order of magnitude faster than the rate of unwinding of the nucleic acid containing 50% cytidine residues (*54*). Thus, the results on the effect of the base composition of the nucleic acid on the rate of NTP hydrolysis greatly corroborate the unwinding studies. By the same token, the type of nucleotide cofactor bound to the helicase will also control the rate of dsDNA unwinding, which will be the fastest in the presence of purine cofactors. Second, the *E. coli* origin of replication, oriC, contains AT-rich regions, specifically recognized by the DnaA protein (*56*). In turn, the formed DnaA−DNA complex is partially unwound to accept the DnaB−DnaC complex. This very specific recognition process requires NTP. Although the mechanism of the recognition process is unknown, our data indicate that it will be accompanied by a dramatic increase in the NTP hydrolysis rate of the DnaB helicase associated with the nucleic acid stretches containing adenosine. In other words, the recognition of the structure of the oriC complex requires a NTPase hydrolysis rate of the DnaB helicase faster than that observed for the free enzyme, or for the enzyme involved in dsDNA unwinding on the DNAs containing a small fraction of adenosine nucleotides. The increase in the NTP hydrolysis rate would be induced through specific activation of the DnaB helicase by adenosine-rich sequences of oriC.

*Free Energy Transduction by the DnaB Helicase−ssDNA Complex*. As we pointed out above, the effect of the ssDNA on the apparent, partial equilibrium constant, $K_1$, is surprisingly smaller than expected from the ground-state thermodynamic studies [companion paper (DOI 10.1021/bi900050x)] (*26*−*29*). However, the temperature effect clearly indicates that the binding step, as seen in the single-turnover experiments, must contain an extra step. Moreover, the step must be energetically costly, thus lowering the observed, apparent binding constant, $K_1$. The simplest explanation of the observed behavior is that this extra step during the NTP binding and hydrolysis is not easily available in the stationary complex, i.e., in the absence of the chemical step. Recall that the kinetic studies of the dsDNA unwinding by the DnaB helicase indicate that the enzyme, which does catalyze NTP hydrolysis, enters a different, catalytic reaction pathway than in the stationary complex, with an increased propensity to dissociate from the DNA (*54*, *55*). Moreover, the helicase needs an "ignition" step prior to the unwinding steps; i.e., it undergoes a transition from the nonproductive to the productive complex. The stationary complex reflexes the events prior to the selection of the catalytic pathway, which includes a dramatic increase in the affinity of the enzyme for the ssDNA, but not necessarily the transition from a nonproductive to productive complex. In the single-turnover studies of NTP hydrolysis, one observes a single catalytic event, corresponding to the first step in the studied unwinding process, which, in turn, contains the transition from a nonproductive to productive complex (*54*, *55*). Thus, the obtained results on NTP hydrolysis strongly suggest that the transition from a nonproductive to productive complex in the unwinding reaction includes a step with a positive free energy change.

Complete elucidation of the free energy transduction mechanism by the DnaB helicase requires further studies. Nevertheless, the obtained data for NTP hydrolysis in the presence and absence of the nucleic acid provide an insight into this mechanism. A characteristic feature of the motor protein is that the free energy change accompanying the NTP hydrolysis in the active site is very small, as compared to the $\Delta G_{ATP}°$ of approximately −7.5 kcal/mol of the free ATP hydrolysis in solution (*57*). For instance, the equilibrium constant describing the ATP ↔ ADP·$P_i$ step in the myosin system is ~10 (*32*, *33*, *44*). A similar low value is observed for the DnaB helicase where, in the case of ATP, the average $K_2$ is ~2.3, indicating that ATP hydrolysis in the active site of the helicase is, on average, accompanied by a $\Delta G_2°$ of approximately −0.5 kcal/mol (*54*, *55*). Accumulation of the chemical free energy by the motor protein, which can then be used in the energy transduction into, for example, a mechanical

one, is achieved through an affinity of ATP orders of magnitude higher than the affinity of ADP (*32*, *33*). The large difference in affinity decreases the chemical potential of ATP in the active site, making the NTP hydrolysis readily reversible and allowing the enzyme to store part of the cofactor binding energy in the complex (*32*, *33*, *44*).

However, the determined ATP binding constant for the helicase−ssDNA complex ($K_{ATP}$), which undergoes ATP hydrolysis, is only $\approx 1 \times 10^5$ $M^{-1}$. This is comparable to the $K_{ADP}$ of $\approx 2 \times 10^5$ $M^{-1}$ obtained in the studies of the stationary complex, and it is not enough to compensate for the $\Delta G_{ATP}°$ of approximately −7.5 kcal/mol of the free ATP hydrolysis (*57*). On the other hand, as discussed above, NTP hydrolysis and dsDNA unwinding studies indicate that the enzyme, undergoing NTP hydrolysis, enters an active catalytic pathway different from that observed for the passive stationary complex. The probability of the cofactor in the stationary complex entering these states must be very low. Moreover, a very fast and efficient dsDNA unwinding reaction strongly suggests that the affinity of ADP for the NTP-binding site of the DnaB helicase is much lower than that observed in the stationary complex, if any at all (*54*, *55*). In other words, in the stationary complex, a different pathway is available for ADP, which practically never enters the intermediate, $(H\text{-}NDP\cdot P_i)_2$, of the NTP hydrolysis (Scheme 1). In the case of ADP, the stationary complex would reflect the events subsequent to the hydrolysis reaction, involved in allosteric control of the interactions with the ssDNA and occurring after the release of the inorganic phosphate from the $(H\text{-}NDP\cdot P_i)_2$ intermediate.

Taking the consideration described above into account, the determined free energy change accompanying binding of ATP to the DnaB−ssDNA complex (20 °C) is then $(\Delta G_{ATP})_B° \approx -RT \ln K_{ATP} \sim -6.7$ kcal/mol. The following ATP hydrolysis contributes only $\Delta G_H° \approx -0.5$ kcal/mol. However, the subsequent conformational transition, $(H\text{-}ADP\cdot P_i)_1 \leftrightarrow (H\text{-}ADP\cdot P_i)_2$, is characterized by an average $K_3$ value of ∼33, in the presence of the ssDNA (Table 1). This step releases approximately −2 kcal/mol ($\Delta G_C°$). In total, approximately −9.2 kcal/mol is released in the process of ATP binding and hydrolysis by the helicase−ssDNA complex, because the enzyme, as a catalyst, does not change the equilibrium of the ATP hydrolysis. Therefore, approximately −9.2 kcal/mol − (−7.5 kcal/mol) = −1.7 kcal/mol of the free energy can accumulate in the DnaB−ssDNA complex, which can be used in energy transduction. The DnaB helicase unwinds a single base pair in a single catalytic event (*54*, *55*). The value of ∼1.7 kcal/mol is just enough to unwind a single base pair of the dsDNA (*59*).

*The Allosteric Signal That Activates the NTP Hydrolysis Comes Predominantly from the Strong DNA-Binding Subsite. The Weak DNA-Binding Subsite Indirectly Modulates the Allosteric Interactions of the Strong Binding Subsite*. Fluorescence emission of the etheno derivatives is predominantly a function of the base mobility and base separation, i.e., the structure of the nucleic acid and much less a function the polarity of the environment of the fluorophore (*34*−*37*). Fluorescence titrations (Figure 9) clearly show a mutual interdependence of the strong and weak DNA-binding subsites of the DnaB helicase. If this were not the case, the relative fluorescence increase of $d\varepsilon A(p\varepsilon A)_9(pT)_{10}$, which has all ethenoadenosines in the strong binding subsite, would be the same as that observed for the $d\varepsilon A(p\varepsilon A)_{19}$ oligomer, i.e., 260% instead of only ∼85%. Thus, the structure of the nucleic acid in the strong subsite is sensitive to the type of nucleic acid bound in the weak subsite.

The observed differences among $dA(pA)_{19}$, $dA(pA)_9(pC)_{10}$, and $dC(pC)_9(pA)_{10}$ in allosterically inducing the increase in the NTP hydrolysis rate constants are dramatic (Figure 10). Notice that the greatest increase in the rates of the chemical step, H-CTP ↔ $(H\text{-}CDP\cdot P_i)_1$, is observed only when the strong allosteric effector, the adenosines, is in the strong DNA-binding subsite, i.e., in the case of $dA(pA)_{19}$ and $dA(pA)_9(pC)_{10}$. These data indicate that the allosteric signal from the total ssDNA-binding site to the NTP-binding site is predominantly, if not exclusively, generated from the strong DNA-binding subsite. Notice that the strong allosteric effector, adenosines, bound in the weak DNA-binding subsite does not induce the maximum increase in $k_2$ and $k_{-2}$, for the same strong effector in the strong DNA-binding subsite, in the case of $dA(pA)_{19}$. Nevertheless, adenosines in the weak subsite, in the case of $dC(pC)_9(pA)_{10}$, can increase the efficiency of the weak effector, cytidines, bound in the strong subsite (Table 1). These data indicate that the two DNA-binding subsites have a nonadditive effect. Similarly, the weak effector, cytidines, in the weak subsite, in the case of $dA(pA)_9(pC)_{10}$, does not act additively but dramatically reinforces the specific strong effect of the adenosines. The same weak effector in the weak DNA-binding subsite is inefficient in inducing a high hydrolysis rate for the weak effector, cytidines, bound in the strong DNA-binding subsite, in the case of $dC(pC)_{19}$ (Table 2). These results indicate that the weak DNA-binding subsite indirectly modulates the allosteric effect of the strong subsite on NTP hydrolysis. Fluorescence titration data (Figure 9) indicate that this happens through structural changes in the nucleic acid fragment bound in the strong DNA-binding subsite.

## ACKNOWLEDGMENT

We thank Gloria Drennan Bellard for reading the manuscript.

## REFERENCES

1. Delagoutte, E., and von Hippel, P. H. (2002) Helicase mechanisms and the coupling of helicases within macromolecular machines. Part I: Structure and properties of isolated helicases. *Q. Rev. Biophys. 35*, 431–478.
2. Delagoutte, E., and von Hippel, P. H. (2003) Helicase mechanisms and the coupling of helicases within macromolecular machines. Part II: Integration of helicases into cellular processes. *Q. Rev. Biophys. 36*, 1–69.
3. Lohman, T. M., and Bjorson, K. P. (1996) Mechanisms of helicase-catalyzed DNA unwinding. *Annu. Rev. Biochem. 65*, 169–214.
4. West, S. C. (1996) DNA helicases: New breeds of translocating motors and molecular pumps. *Cell 86*, 177–180.
5. Enemark, E. J., and Joshua-Tor, L. (2008) On Helicases and Other Motor Proteins. *Curr. Opin. Struct. Biol. 18*, 243–257.
6. LeBowitz, J. H., and McMacken, R. (1986) The *Escherichia coli* dnaB Replication Protein Is a DNA Helicase. *J. Biol. Chem. 261*, 4738–4748.
7. Baker, T. A., Funnell, B. E., and Kornberg, A. (1987) Helicase Action of dnaB Protein During Replication from the *Escherichia coli* Chromosomal Origin *in Vitro*. *J. Biol. Chem. 262*, 6877–6885.
8. Kornberg, A., and Baker, T. A. (1992) DNA Replication , pp 355−378, Freeman, San Francisco.
9. Marians, K. J. (1992) Prokaryotic DNA replication. *Annu. Rev. Biochem. 61*, 673–719.
10. Bujalowski, W. (2003) Expanding the Physiological Role of the Hexameric Helicases. *Trends Biochem. Sci. 28*, 116–118.
11. Arai, K., and Kornberg, A. (1981) Mechanism of dnaB protein action. III. Allosteric role of ATP in the alteration of DNA structure by dnaB protein in priming replication. *J. Biol. Chem. 256*, 5260–5266.
12. Arai, K.-I., and Kornberg, A. (1981) Mechanism of *dnaB* Protein Action. IV. General Priming of DNA Replication by *dnaB* Protein and Primase Compared with RNA Polymerase. *J. Biol. Chem. 256*, 5267–5272.
13. Tongu, K., Peng, H., and Marians, K. J. (1994) Identification of a Domain of *E. coli* Primase Required for Functional Interaction with the DnaB Helicase at the Replication Fork. *J. Biol. Chem. 269*, 4675–4682.

14. Doran, K. S., Helinski, D. R., and Konieczny, I. (1999) A critical DnaB Box Directs the Cooperative Binding of the *Escherichia coli* DnaB to the Plasmide RK2 Replication. *J. Biol. Chem. 274*, 17918–17923.
15. Reha-Krantz, L. J., and Hurwitz, J. (1978) The *dnaB* Gene Product of *Escherichia coli*, I. Purification, Homogeneity, and Physical Properties. *J. Biol. Chem. 253*, 4043–4050.
16. Bujalowski, W., Klonowska, M. M., and Jezewska, M. J. (1994) Oligomeric Structure of *Escherichia coli* Primary Replicative Helicase DnaB Protein. *J. Biol. Chem. 269*, 31350–31358.
17. Jezewska, M. J., and Bujalowski, W. (1996) Global Conformational Transitions in *E. coli* Primary Replicative DnaB Protein Induced by ATP, ADP and Single-Stranded DNA Binding. *J. Biol. Chem. 271*, 4261–4265.
18. Bujalowski, W., and Jezewska, M. J. (1995) Interactions of *Escherichia coli* Primary Replicative Helicase DnaB Protein with Single-Stranded DNA. The Nucleic Acid Does Not Wrap Around the Protein Hexamer. *Biochemistry 34*, 8513–8519.
19. Jezewska, M. J., Kim, U.-S., and Bujalowski, W. (1996) Binding of *Escherichia coli* Primary Replicative Helicase DnaB Protein to Single-Stranded DNA. Long-Range Allosteric Conformational Changes within the Protein Hexamer. *Biochemistry 35*, 2129–2145.
20. Jezewska, M. J., Kim, U.-S., and Bujalowski, W. (1996) Binding of *Escherichia coli* Primary Replicative Helicase DnaB Protein to Single-Stranded DNA. Long-Range Allosteric Conformational Changes within the Protein Hexamer. *Biochemistry 35*, 2129–2145.
21. Jezewska, M. J., and Bujalowski, W. (1996) A General Method of Analysis of Ligand Binding to Competing Macromolecules Using the Spectroscopic Signal Originating from a Reference Macromolecule. Application to *Escherichia coli* Replicative Helicase DnaB Protein-Nucleic Acid Interactions. *Biochemistry 35*, 2117–2128.
22. Jezewska, M. J., Rajendran, S., and Bujalowski, W. (1997) Strand Specificity in the Interactions of *Escherichia coli* Primary Replicative Helicase DnaB Protein with Replication Fork. *Biochemistry 36*, 10320–10326.
23. Jezewska, M. J., Rajendran, S., and Bujalowski, W. (1998) Complex of *Escherichia coli* Primary Replicative Helicase DnaB Protein with a Replication Fork. Recognition and Structure. *Biochemistry 37*, 3116–3136.
24. Jezewska, M. J., Rajendran, S., Bujalowska, D., and Bujalowski, W. (1998) Does ssDNA Pass Through the Inner Channel of the Protein Hexamer in the Complex with the *E. coli* DnaB Helicase? Fluorescence Energy Transfer Studies. *J. Biol. Chem. 273*, 10515–10529.
25. Jezewska, M. J., Rajendran, S., and Bujalowski, W. (1998) Functional and Structural Heterogeneity of the DNA Binding of the *E. coli* Primary Replicative Helicase DnaB protein. *J. Biol. Chem. 273*, 9058–9069.
26. Bujalowski, W., and Klonowska, M. M. (1993) Negative Cooperativity in the Binding of Nucleotides to *Escherichia coli* Replicative Helicase DnaB Protein. Interactions with Fluorescent Nucleotide Analogs. *Biochemistry 32*, 5888–5900.
27. Bujalowski, W., and Klonowska, M. M. (1994) Close Proximity of Tryptophan Residues and ATP-Binding Site in *Escherichia coli* Primary Replicative Helicase DnaB Protein. Molecular Topography Studies. *J. Biol. Chem. 269*, 31359–31371.
28. Bujalowski, W., and Klonowska, M. M. (1994) Structural Characteristics of the Nucleotide Binding Site of the *E. coli* primary replicative Helicase DnaB Protein. Studies with Ribose and Base-Modified Fluorescent Nucleotide Analogs. *Biochemistry 33*, 4682–4694.
29. Jezewska, M. J., Kim, U.-S., and Bujalowski, W. (1996) Interactions of *Escherichia coli* Primary Replicative Helicase DnaB Protein with Nucleotide Cofactors. *Biophys. J. 71*, 2075–2086.
30. Bujalowski, W., and Jezewska, M. J. (2000) Kinetic Mechanism of Nucleotide Cofactor Binding to *Escherichia coli* Replicative Helicase DnaB Protein. Stopped-Flow Kinetic Studies Using Fluorescent, Ribose-, and Base-Modified Nucleotide Analogs. *Biochemistry 39*, 2106–2122.
31. Rajendran, S., Jezewska, M. J., and Bujalowski, W. (2000) Multiple-step Kinetic Mechanism of DNA-independent ATP Binding and Hydrolysis by *Escherichia coli* Replicative Helicase DnaB Protein: Quantitative Analysis Using the Rapid Quench-Flow Method. *J. Mol. Biol. 303*, 773–795.
32. Jencks, W. P. (1980) The Utilization of Binding Energy in Coupled Vectorial Processes. *Adv. Enzymol. 51*, 75–106.
33. Bagshaw, C. R., and Trentham, D. R. (1974) The Characterization of Myosin-Product Complexes and of Product-Release Steps during the Magnesium Ion-Dependent Adenosine Triphosphatase Reaction. *Biochem. J. 141*, 331–349.
34. Ledneva, R. K., Razjivin, A. P., Kost, A. A., and Bogdanov, A. A. (1977) Interaction of tobacco mosaic virus protein with synthetic polynucleotides containing a fluorescent label: Optical properties of poly(A,$\varepsilon$A) and poly(C,eC) copolymers and energy migration from the tryptophan to 1,$N^6$-ethenoadenosine or 3,$N^4$-ethenocytosine residues in RNP. *Nucleic Acids Res. 5*, 4226–4243.
35. Secrist, J. A., Bario, J. R., Leonard, N. J., and Weber, G. (1972) Fluorescent Modification of Adenosine-Containing Coenzymes. Biological Activities and Spectroscopic Properties. *Biochemistry 11*, 3499–3506.
36. Baker, B. M., Vanderkooi, J., and Kallenbach, N. R. (1978) Base Stacking in a Fluorescent Dinucleotiside Monophosphate: $\varepsilon$Ap$\varepsilon$A. *Biopolymers 17*, 1361–1372.
37. Tolman, G. L., Barrio, J. R., and Leonard, N. J. (1974) Chloroacetaldehyde-Modified Dinucleoside Phosphates. Dynamic Fluorescence Quenching and Quenching due to Intramolecular Complexation. *Biochemistry 13*, 4869–4878.
38. Johnson, K. A. (1995) Rapid quench kinetic analysis of polymerases, adenosinetriphosphatases, and enzyme intermediates. *Methods Enzymol. 249*, 38–61.
39. Bernasconi, C. F. (1976) Relaxation Kinetics , Academic Press, New York.
40. Bujalowski, W., and Jezewska, M. J. (2000) Kinetic Mechanism of the Single-Stranded DNA Recognition by *Escherichia coli* Replicative Helicase DnaB Protein. Application of the Matrix Projection Operator Technique to Analyze Stopped-Flow Kinetics. *J. Mol. Biol. 295*, 831–852.
41. Bujalowski, W. (2006) Thermodynamic and Kinetic Methods of Analyses of Protein−Nucleic Acid Interactions. From Simpler to More Complex Systems. *Chem. Rev. 106*, 556–606.
42. Gutfreund, H. (1995) Kinetics for the Life Sciences , pp 197−224, Cambridge University Press, Cambridge, U.K.
43. Hammes, G. G., and Schimmel, P. R. (1970) The Enzymes. Kinetics and Mechanism , Vol. II, pp 67−114, Academic Press, New York.
44. Abeles, R. H., Frey, P. A., and Jencks, W. P. (1992) Biochemistry , pp 791−822, Jones & Bartlett.
45. Jezewska, M. J., Galletto, R., and Bujalowski, W. (2004) Interactions of the RepA helicase hexamer of plasmid RSF1010 with the ssDNA. Quantitative Analysis of Stoichiometries, Intrinsic Affinities, Cooperativities, and Heterogeneity of the Total ssDNA-binding Site. *J. Mol. Biol. 343*, 115–136.
46. Jezewska, M. J., Bujalowski, P. J., and Bujalowski, W. (2007) Interactions of the DNA Polymerase X of African Swine Fever Virus With Double-Stranded DNA. Functional Structure of the Complex. *J. Mol. Biol. 373*, 75–95.
47. Lucius, A. L., Jezewska, M. J., and Bujalowski, W. (2006) The *Escherichia coli* PriA Helicase Has Two Nucleotide-Binding Sites Differing in Their Affinities for Nucleotide Cofactors. I. Intrinsic Affinities, Cooperativities, and Base Specificity of Nucleotide Cofactor Binding. *Biochemistry 45*, 7202–7216.
48. Marcinowicz, A., Jezewska, M. J., and Bujalowski, W. (2008) Multiple Global Conformational States of the Hexameric RepA Helicase of Plasmid RSF1010 With Different ssDNA-Binding Capabilities Are Induced By Different Numbers of Bound Nucleotides. Analytical Ultracentrifugation and Dynamic Light Scattering Studies. *J. Mol. Biol. 375*, 386–408.
49. Yu, X., Jezewska, M. J., Bujalowski, W., and Egelman, E. H. (1996) The hexameric *E. coli* DnaB helicase can exist in different quaternary states. *J. Mol. Biol. 259*, 7–14.
50. Yang, S., Yu, X., Van Loock, M. S., Jezewska, M. J., Bujalowski, W., and Egelman, E. H. (2002) Flexibility of the Rings: Structural Asymmetry in the DnaB Hexameric Helicase. *J. Mol. Biol. 321*, 839–849.
51. Moore, J. W., and Pearson, R. G. (1981) Kinetics and Mechanism, pp 235−283, John Wiley & Sons, New York.
52. de Meis, L. (1985) Role of Water in Processes of Energy Transduction: $Ca^{2+}$-transport ATPase and inorganic pyrophosphatase. *Biochem. Soc. Symp. 50*, 97–125.
53. Dupont, Y., and Pougeois, R. (1983) Evaluation of $H_2O$ activity in the free or phosphorylated catalytic site of $Ca^{2+}$-ATPase. *FEBS Lett. 156*, 93–98.
54. Galletto, R., Jezewska, M. J., and Bujalowski, W. (2004) Unzipping Mechanism of the Double-Stranded DNA Unwinding by a Hexameric Helicase. Quantitative Analysis of the Rate of the dsDNA Unwinding, Processivity and Kinetic Step-Size of the *Escherichia coli* DnaB Helicase Using Rapid Quench-Flow Method. *J. Mol. Biol. 343*, 83–99.

55. Galletto, R., Jezewska, M. J., and Bujalowski, W. (2004) Unzipping Mechanism of the Double-Stranded DNA Unwinding by a Hexameric Helicase. The Effect of the 3′ Arm and the Stability of the dsDNA on the Unwinding Activity of the *Escherichia coli* DnaB Helicase. *J. Mol. Biol. 343*, 101–114.
56. Margulies, C., and Kaguni, J. M. (1996) Ordered and Sequential Binding of DnaA Protein to *oriC*, the Chromosomal Origin of *Escherichia coli*. *J. Biol. Chem. 271*, 17035–17040.
57. Klotz, I. M. (1967) Energy Changes in Biochemical Reactions , pp 52−60, Academic Press, New York.
58. Nakayama, N., Arai, N., Kazior, Y., and Arai, K.-I. (1984) Structural and Functional Studies of the *dnaB* Protein Using Limited Proteolysis. *J. Biol. Chem. 259*, 88–96.
59. Cocco, S., Monasson, R., and Marko, J. F. (2001) Force and Kinetic Barriers to unzipping of the DNA Double Helix. *Proc. Natl. Acad. Sci. U.S.A. 98*, 8608–8613.